Schwarz, T.F., Werner, T., Schatzl, H.M., 1999. Analysis of 27 mammalian and 9 avian PrPs reveals high conservation of flexible regions of the prion protein. J. Mol. Biol. 289, 1163–1178.

Yokoyama, T., Kimura, K.M., Ushiki, Y., Yamada, S., Morooka, A., Nakashiba, T., Sassa, T., Itohara, S., 2001. In vivo conversion of cellular prion protein to pathogenic isoforms, as monitored by conformation-specific antibodies. J. Biol. Chem. 276, 11265–11271.

Zanusso, G., Liu, D., Ferrari, S., Hegyi, I., Yin, X., Aguzzi, A., Hornemann, S., Liemann, S., Glockshuber, R., Manson, J.C., Brown, P., Petersen, R.B., Gambetti, P., Sy, M.S., 1998. Prion protein expression in different species: analysis with a panel of new mAbs. Proc. Natl. Acad. Sci. U.S.A. 95, 8812–8816.

Zhang, H., Kaneko, K., Nguyen, J.T., Livshits, T.L., Baldwin, M.A., Cohen, F.E., James, T.L., Prusiner, S.B., 1995. Conformational transitions in peptides containing two putative alpha-helices of the prion protein. J. Mol. Biol. 250, 514–526.

Journal of General Virology (2004), 85, 3473–3482 DOI 10.1099/vir.0.80113-0

Cell-surface retention of PrP^C by anti-PrP antibody prevents protease-resistant PrP formation

Chan-Lan Kim,[1] Ayako Karino,[1] Naotaka Ishiguro,[1] Morikazu Shinagawa,[1]† Motoyoshi Sato[2] and Motohiro Horiuchi[1]‡

Correspondence
Motohiro Horiuchi
horiuchi@vetmed.hokudai.ac.jp

Laboratory of Veterinary Public Health[1] and Laboratory of Veterinary Radiology[2], Obihiro University of Agriculture and Veterinary Medicine, Inada-cho, Obihiro, Hokkaido 080-8555, Japan

The C-terminal portion of the prion protein (PrP), corresponding to a protease-resistant core fragment of the abnormal isoform of the prion protein (PrP^{Sc}), is essential for prion propagation. Antibodies to the C-terminal portion of PrP are known to inhibit PrP^{Sc} accumulation in cells persistently infected with prions. Here it was shown that, in addition to monoclonal antibodies (mAbs) to the C-terminal portion of PrP, a mAb recognizing the octapeptide repeat region in the N-terminal part of PrP that is dispensable for PrP^{Sc} formation reduced PrP^{Sc} accumulation in cells persistently infected with prions. The 50 % effective dose was as low as ~1 nM, and, regardless of their epitope specificity, the inhibitory mAbs shared the ability to bind cellular prion protein (PrP^C) expressed on the cell surface. Flow cytometric analysis revealed that mAbs that bound to the cell surface during cell culture were not internalized even after their withdrawal from the growth medium. Retention of the mAb–PrP^C complex on the cell surface was also confirmed by the fact that internalization was enhanced by treatment of cells with dextran sulfate. These results suggested that anti-PrP mAb antagonizes PrP^{Sc} formation by interfering with the regular PrP^C degradation pathway.

Received 16 March 2004
Accepted 26 July 2004

INTRODUCTION

Transmissible spongiform encephalopathies (TSEs), also called prion diseases, are fatal neurodegenerative diseases and include scrapie in sheep and goats, bovine spongiform encephalopathy and Creutzfeldt–Jakob disease (CJD) in humans. The causative agent of TSEs, often called a prion, is composed mainly of an abnormal isoform (PrP^{Sc}) of the host cellular prion protein (PrP^C). Mice with genetic knockout of the PrP gene are resistant to prion disease (Bueler *et al.*, 1993) and neurons lacking PrP^C expression are resistant to degeneration, regardless of the presence of PrP^{Sc} (Mallucci *et al.*, 2003). Thus, PrP^C is essential for prion propagation and pathogenesis.

Conversion of PrP^C to PrP^{Sc} is believed to involve direct interaction of the two PrP isoforms. Although the molecular mechanism of conversion is not yet fully understood, it is known that mature PrP^C expressed on the cell surface is a substrate for PrP^{Sc} formation, and a process that involves a conformational transformation takes place in subcellular compartments associated with the degradation pathway of PrP^C, including a sphingolipid-rich membrane microdomain, called a lipid raft (Caughey & Raymond, 1991; Naslavsky *et al.*, 1997; Vey *et al.*, 1996).

Because of the emergence of variant CJD and iatrogenic CJD by dura matter transplantation, especially in Japan, the establishment of therapeutics for prion disease is urgently needed. Therapeutics have been directed at the binding of the two PrP isoforms, as well as the process of conformational transformation, since the conversion of PrP^C to PrP^{Sc} is associated with neuronal pathogenicity. To date, many substances have been reported to inhibit PrP^{Sc} formation in cell culture and/or cell-free systems, including amyloid-binding dyes (Caughey & Race, 1992), sulfated glycosaminoglycans (Caughey & Raymond, 1993), tetrapyrrole compounds (Caughey *et al.*, 1998), cysteine protease inhibitors (Doh-Ura *et al.*, 2000), substituted tricyclic derivatives such as chlorpromazine and quinacrine (Doh-Ura *et al.*, 2000; Korth *et al.*, 2001), branched polyamines (Supattapone *et al.*, 1999, 2001), peptides (Chabry *et al.*, 1998; Soto *et al.*, 2000) and conversion-incompetent PrP (Holscher *et al.*, 1998; Horiuchi *et al.*, 2000; Kaneko *et al.*, 1997). Some of these have already been examined *in vivo*. For instance, sulfated glycosaminoglycans and tetrapyrrole compounds were effective when administered at early stages of infection or simultaneously with the scrapie-affected brain inoculum (Ehlers & Diringer, 1984; Ladogana

†Present address: Prion Disease Research Center, National Institute of Animal Health, Kannondai, Tsukuba, Ibaragi, 305-0856, Japan.

‡Present address: Laboratory of Prion Diseases, Graduate School of Veterinary Medicine, Hokkaido University, Kita 18, Nishi 9, Kita-ku, Sapporo 060-0818, Japan.

et al., 1992; Priola *et al.*, 2000). Polyene antibiotics prolonged the incubation period, even when administered at the middle-late stage of infection (Demaimay *et al.*, 1997), but the effects appeared to depend on the prion strains and host animals studied (Demaimay *et al.*, 1999; Xi *et al.*, 1992). Recently, Doh-Ura and colleagues (2004) showed that intraventricular administration of pentosan polysulfate and quinine prolonged the incubation periods in a prion-infected transgenic mouse model, even at a late stage of infection (Doh-Ura *et al.*, 2004; Murakami-Kubo *et al.*, 2004). Further *in vivo* studies are expected to lead to the establishment of effective therapeutics for prion diseases. However, to achieve more efficient therapeutics, it is essential to elucidate the mechanisms of action and to investigate proper delivery of drugs based on pharmacokinetics.

Anti-PrP antibodies have also been reported to inhibit the formation of PrP^{Sc} in cultured cells and/or cell-free systems (Enari *et al.*, 2001; Horiuchi & Caughey, 1999; Kaneko *et al.*, 1995; Peretz *et al.*, 2001). Transgenic mice expressing an anti-PrP mAb on B cells (Heppner *et al.*, 2001), immunization with recombinant PrP (Sigurdsson *et al.*, 2002) and passive immunization with an anti-PrP mAb (White *et al.*, 2003) antagonized the peripheral inoculation of scrapie-affected brain inoculum. These *in vivo* experiments suggested the possible use of anti-PrP antibodies as a therapy for prion diseases. However, it remains unclear how anti-PrP antibodies can antagonize PrP^{Sc} formation in cells. To address this point, in the current study, we evaluated a panel of anti-PrP mAbs against diverse epitopes for inhibition of PrP^{Sc} formation. We found that a mAb recognizing the octapeptide repeat sequence, a region that is not essential for PrP^{Sc} formation, reduced PrP^{Sc} accumulation in cells persistently infected with prions. Furthermore, our data suggest a possible link between cell-surface retention of PrP^{C} by anti-PrP antibodies and inhibition of PrP^{Sc} formation in cells.

METHODS

Antibodies and chemicals. The properties of anti-PrP mAbs used in this study have been described elsewhere (Kim *et al.*, 2004). The mAb against sarcomeric actin (clone alpha-Sr-1) was purchased from DAKO. Stock solutions of chlorpromazine, dextran sulfate 500 (DS500) and polyethyleneimine were prepared in deionized water, while E-64d was dissolved in DMSO and quinacrine in methanol. Culture medium containing each chemical compound or mAb was prepared freshly for each experiment.

Cell culture. The mouse neuroblastoma cell line Neuro2a (CCL-131; ATCC) was cultured in Dulbecco's modified Eagle's medium (ICN Biomedicals) with 10% fetal bovine serum (FBS) and non-essential amino acids. Mouse neuroblastoma cells persistently infected with prions, originally established by Race *et al.* (1987), were cloned by limiting dilution. Subclone I3/I5-9, which possessed a high level of PrP^{Sc}, was used in this study. I3/I5-9 cells were maintained in Opti-MEM (Invitrogen) containing 10% FBS and cells passaged fewer than 20 times were used for experiments.

Treatment of cells persistently infected with prions and sample preparation. Almost-confluent I3/I5-9 cells in 25 cm^2 flasks were split 1:20 into 35 mm tissue culture dishes. On day 2, the medium was replaced with 3 ml Opti-MEM containing 4% FBS and each test compound or mAb, and the cells were cultured for a further 3 days. For PrP^{C} detection, the cells were washed with PBS and lysed with 300 µl lysis buffer A (1% Zwittergent 3-14, 150 mM NaCl, 50 mM Tris/HCl, pH 7·5) supplemented with protease inhibitors (2 mM EDTA, 1 µg pepstatin ml^{-1}, 2 µg leupeptin ml^{-1}, 2 µM bestatin and 1 µg aprotinin ml^{-1}). After the removal of cell debris by low-speed centrifugation, samples were centrifuged at 45 000 r.p.m. for 30 min at 4 °C using the TLA 100.3 rotor of a Beckman Optima TLX and the resulting supernatants were used as a source of PrP^{C}. For the detection of PrP^{Sc}, cells were lysed with 300 µl lysis buffer B (5 mM EDTA, 0·5% Triton X-100, 0·5% sodium deoxycholate, 150 mM NaCl, 10 mM Tris/HCl, pH 7·5) and kept on ice for 30 min. Cell debris was removed by centrifugation for 5 min at 1000 r.p.m. A portion of the sample (10%) was removed for determination of protein concentration using the DC protein assay (Bio-Rad) and the remaining portions were treated with 20 µg proteinase K ml^{-1} for 20 min at 37 °C. Proteolysis was terminated by the addition of 1 mM Pefabloc (Roche). The samples were then treated with DNase I (100 µg ml^{-1}) and RNase A (5 µg ml^{-1}) for 15 min at room temperature and centrifuged at 70 000 r.p.m. for 2 h at 4 °C using the TLA 100.3 rotor of a Beckman Optima TLX. The resulting pellets were dissolved in SDS-PAGE sample buffer.

SDS-PAGE and immunoblotting. SDS-PAGE was carried out using NuPAGE 12% Bis-tris gels and MOPS-SDS running buffer according to the manufacturer's instructions (Invitrogen). After SDS-PAGE, proteins were transferred on to Immobilon-P PVDF membranes (Millipore) using a Transblot Mini Cell wet-type blotting apparatus (Bio-Rad) and NuPAGE transfer buffer (Invitrogen) at 60 V for 2 h. Immunoreactive proteins were detected using X-ray film as described elsewhere (Kim *et al.*, 2004). For quantitative analysis, immunoreactive proteins were visualized using the Western-Star Protein detection kit (TROPIX) according to the supplier's instructions and processed with an LAS-1000 lumino image analyser (Fujifilm). The intensity of the bands was quantified using Science Lab 98 Image Gauge software (Fujifilm).

Flow cytometric analysis. Adherent cells were treated with ice-cold PBS containing 0·1% collagenase (Wako) and dispersed by pipetting. Cells were washed with 0·5% FBS in PBS (FBS/PBS) and incubated with anti-PrP mAbs diluted with 0·5% FBS/PBS for 30 min on ice. Cells were washed three times with 0·5% FBS/PBS and incubated with 1:2000-diluted Alexa 488-labelled Fab fragment of goat anti-mouse IgG (Molecular Probes) for 30 min. After washing, cells were stained with 5 µg propidium iodide ml^{-1} in 0·5% FBS/PBS for 5 min and analysed using an EPICS XL-ADC flow cytometer (Beckman Coulter). All procedures were carefully carried out under chilled conditions.

Indirect immunofluorescence assay. Cells grown in eight-well slides (Nunc) were fixed with 100% methanol for 20 min at −20 °C. Fixed cells were blocked with 5% FBS/PBS for 30 min at room temperature, after which they were incubated with hybridoma supernatants or mAbs diluted in 1% FBS/PBS for 30 min at room temperature. After washing with PBS, cells were incubated with 1:1000-diluted Alexa 488-labelled Fab fragment of goat anti-mouse IgG for 30 min. Finally, the slides were mounted with PBS containing 50% glycerol and 1% n-propyl gallate (Wako) and examined using a fluorescence microscope equipped with a cooled CCD unit (*Cool*SNAP HQ; Roper).

Cell growth and cytotoxicity. The effect of mAbs on cell growth was analysed using the 4-[3-(4-iodophenyl)-2-(4-nitrophenyl)-2H-5-tetrazolio]-1,3-benzene disulfonate (WST-1) assay (Ishiyama *et al.*, 1996) and cytotoxicity was analysed by lactate dehydrogenase (LDH) release assay using the LDH-Cytotoxic Test (Wako).

RESULTS

Anti-PrP mAbs inhibit PrP^{Sc} accumulation in cultured cells

Several antibodies recognizing regions in the C-terminal portion of PrP have been reported to inhibit PrP^{Sc} accumulation in neuroblastoma cells persistently infected with prions (Enari *et al.*, 2001; Peretz *et al.*, 2001). We recently established a panel of diverse anti-PrP mAbs including those recognizing the octapeptide repeat in the N-terminal region of PrP (Kim *et al.*, 2004). In the current studies, we investigated whether they would effect PrP^{Sc} accumulation in prion-infected neuroblastoma cells. Fig. 1(a) shows the effect of mAbs recognizing linear epitopes on PrP^{Sc} accumulation in I3/I5-9 cells persistently infected with prions. Following a 3-day treatment, only two mAbs reduced PrP^{Sc} accumulation: 31C6, which recognizes aa 143–149 of mouse PrP, and 110, which recognizes PHGGGWG at aa 59–65 and aa 83–89 in the octapeptide repeat. Quantitative analysis revealed that other mAbs did not affect the total amount of PrP^{Sc}, or the ratio of di-, mono- and non-glycosylated PrP^{Sc}.

Flow cytometric analysis showed that mAbs 110 and 31C6 bound PrP^{C} on the cell surface, although the fluorescence intensity of mAb 110 was weaker than that of mAb 31C6 (Fig. 1b, left panel). In contrast, mAbs that had no effect on PrP^{Sc} accumulation did not appear to bind to PrP^{C} on the cell surface (Fig. 1b, right panel). Two other mAbs, 44B1 and 72, which are thought to recognize discontinuous epitopes (Kim *et al.*, 2004), reacted with PrP^{C} on the cell surface (Fig. 1b) and inhibited PrP^{Sc} accumulation (Fig. 2). These results suggested that mAbs that can bind to PrP^{C} on the cell surface have the potential to antagonize PrP^{Sc} accumulation in cells persistently infected with prions.

Fig. 2 shows the dose-dependence of the effect of the anti-PrP mAbs. The four effective mAbs (110, 31C6, 44B1 and 72) reduced the amount of PrP^{Sc} in a dose-dependent manner, although PrP^{Sc} was not completely eliminated following the 3-day treatment. The 50% effective dose (EC_{50}) of mAbs 110, 31C6, 44B1 and 72 was estimated to be 0·2 μg ml^{-1}(1·2 nM), 0·1 μg ml^{-1} (0·7 nM), 0·3 μg ml^{-1} (1·7 nM) and 0·6 μg ml^{-1} (4·1 nM), respectively (Fig. 2b).

Fig. 3 shows the long-term effect of mAbs on PrP^{Sc} formation. Treatment for 6 days with mAb 110, 44B1, 31C6 (Fig. 3) or 72 (data not shown) reduced PrP^{Sc} to an almost undetectable level, and no re-emergence of PrP^{Sc} was observed in the following 6 and 12 days of incubation in the absence of mAbs. On the contrary, mAbs that did not bind to cell-surface PrP^{C} showed little effect on PrP^{Sc} accumulation even after long-term treatment.

The influence of mAbs on cell growth and acute toxicity was examined by WST-1 assay and LDH release assay, respectively. No significant effect on cell growth was observed, even with long-term treatment (5 μg ml^{-1} for 6 days) and mAbs did not demonstrate any acute toxicity (10 μg ml^{-1}) following 2 h of treatment.

Effect of anti-PrP mAbs on total amount of PrP^{C}

Fig. 1(a, lower panel) shows total PrP^{C} in the I3/I5-9 cells treated with mAbs for 3 days. The intensities of PrP^{C} bands were normalized with α-sarcomeric actin on the same blot and PrP^{C} levels relative to cells treated with negative control mAb (P1-284) are indicated at the bottom. Although there was a certain degree of variation, no marked difference was observed in the total amount of PrP^{C}. In contrast, after long-term treatment (6 days), the total amount of PrP^{C} in I3/I5-9 cells treated with mAb 110 or 44B1 appeared to be higher than that with the negative-control mAb or other anti-PrP mAbs (Fig. 3, top right panel). To confirm this further, we repeated the same experiment at least three times for the four inhibitory mAbs, 110, 31C6, 44B1 and 72. Relative PrP^{C} levels in cells treated with these four mAbs were 168±38, 88±23, 183±54 and 103±33%, respectively. These results suggested that the effect of mAbs on PrP^{C} level varied depending on the mAb: mAbs 110 and 44B1 increased total PrP^{C} levels following long-term treatment, while mAbs 31C6 and 72 did not affect the total PrP^{C} level.

Cell-surface localization of the mAb–PrP^{C} complex

The N-terminal portion of PrP, including the octapeptide repeat, is not essential for PrP^{Sc} formation and/or prion propagation (Flechsig *et al.*, 2000; Rogers *et al.*, 1993). The finding that not only the mAbs recognizing the C-terminal part of PrP, such as 31C6 and 44B1, but also mAb 110 inhibited PrP^{Sc} accumulation in the neuroblastoma cells, together with the fact that only the mAbs that bound to cell-surface PrP^{C} showed an inhibitory effect, implied that the mAb–PrP^{C} interaction on the cell surface is essential for inhibition of PrP^{Sc} accumulation. To investigate this further, we analysed the dynamics of anti-PrP mAbs after their binding to the cell surface (Fig. 4). Neuro2a cells were treated with 10 μg mAb 31C6 ml^{-1} for 1 h, after which the cells were cultured for an additional 4 h without mAb. Cells were then harvested and stained with an Alexa 488-conjugated secondary antibody. As a control, cells cultured with mAb 31C6 for 1 h were immediately stained with the secondary antibody. Flow cytometric analysis showed no difference in fluorescence intensity between the two preparations, suggesting that the mAb–PrP^{C} complex remained on the cell surface, even after the additional 4 h culture in the absence of mAb. As I3/I5-9 cells are established by repeated limiting dilution, Neuro2a cells may not be a suitable uninfected control for I3/I5-9 cells. Hence, we carried out the same experiment using I3/I5-9 cells. It is known that elimination of PrP^{Sc} parallels the reduction of prion infectivity. Considering biosafety issues, we used I3/I5-9 cells cured of PrP^{Sc} by long-term treatment with mAb 44B1 for flow cytometric analysis. mAb 31C6 (Fig. 4) and

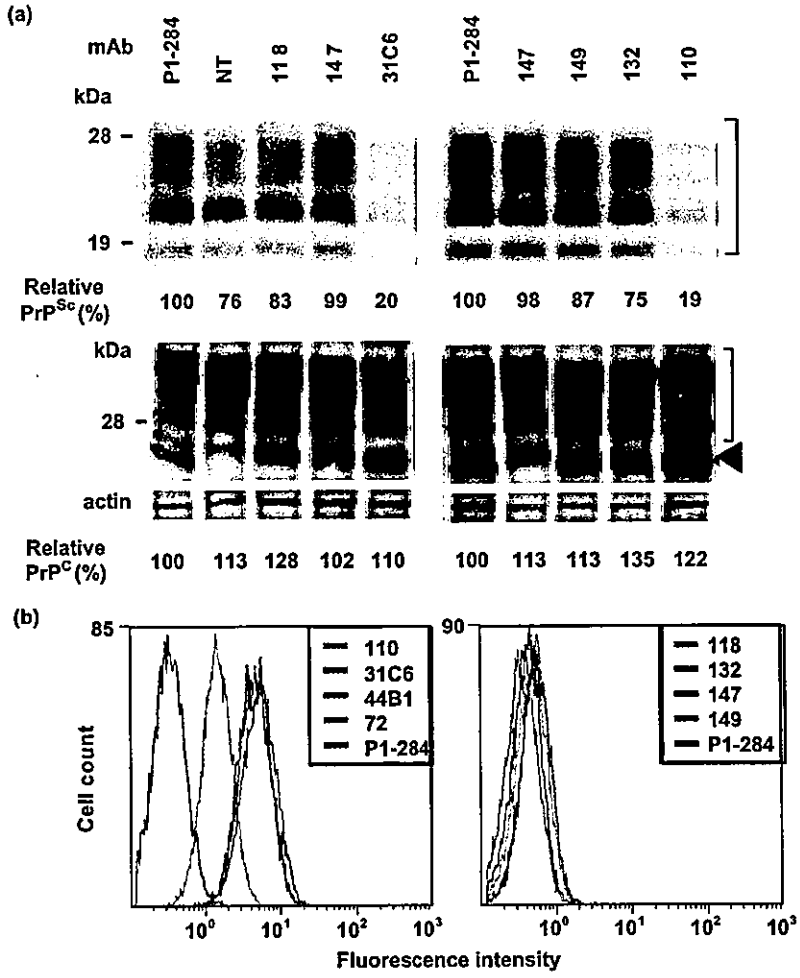

Fig. 1. Inhibition of PrP^{Sc} accumulation in prion-infected I3/I5-9 cells by anti-PrP mAbs. (a) Detection of PrP^{Sc} (upper panels) and PrP^{C} (lower panels). I3/I5-9 cells were cultured for 3 days with 4 % FBS in Opti-MEM containing 5 μg mAbs ml^{-1}. The level of PrP^{Sc} in the cells was determined by immunoblot analysis using mAb 44B1. Antibodies added to the culture are indicated above the panels. mAb P1-284 against feline panleukopenia virus was used as a control for non-specific effects. For detection of PrP^{Sc}, the load volume of each sample was adjusted based on the protein concentration of the corresponding cell lysate that had not been treated with proteinase K. For quantitative analysis of PrP^{Sc}, the three PrP^{Sc} bands indicated by a square bracket (right-hand side, upper panels) were grouped together. To check the ratios of the three PrP^{Sc} bands, each was selected separately. For PrP^{C}, the PrP^{C} bands indicated by a square bracket (right-hand side, lower panels) were quantified. The bands indicated by the arrowhead were excluded from the quantitative analysis, as they overlapped with immunoglobulin light chains that were detected by secondary antibodies. The blot used for PrP^{C} detection was also probed with anti-sarcomeric actin mAb for normalization. The levels of PrP^{Sc} and PrP^{C} relative to cells treated with negative-control mAb (P1-284) are indicated below the panels. NT, cells cultured without mAbs. Molecular mass markers are shown in kDa on the left. Epitopes for mAbs were as follows: 110, aa 56–89; 132, aa 119–127; 118, aa 137–143; 31C6, aa 143–149; 149, aa 147–151; 147, aa 219–229 (Kim *et al.*, 2004). (b) Binding of mAbs to the surface of Neuro2a cells examined by flow cytometry. The left panel shows mAbs that bound to the cell surface, while the right panel shows mAbs that did not bind. mAb P1-284 was used as a control for non-specific binding.

the three other inhibitory mAbs, 110, 44B1 and 72 (data not shown), showed the same retention of mAb–PrP^{C} complexes as observed with Neuro2a cells.

To confirm further the retention of mAb–PrP^{C} complexes on the cell surface, Neuro2a and I3/I5-9 cells were cultured for 1 h with mAbs 110, 31C6, 44B1 and 72, and, in some cases, the cells were cultured for an additional 4 h with mAb-free medium. The cells were then fixed with ice-cold methanol and mAb–PrP^{C} complexes were detected using secondary antibody (Fig. 5). All mAbs bound to the cell surface (Fig. 5a–e) and membrane staining could be detected, even after 4 h incubation in the absence of mAbs (Fig. 5f–j). To characterize further the retention of

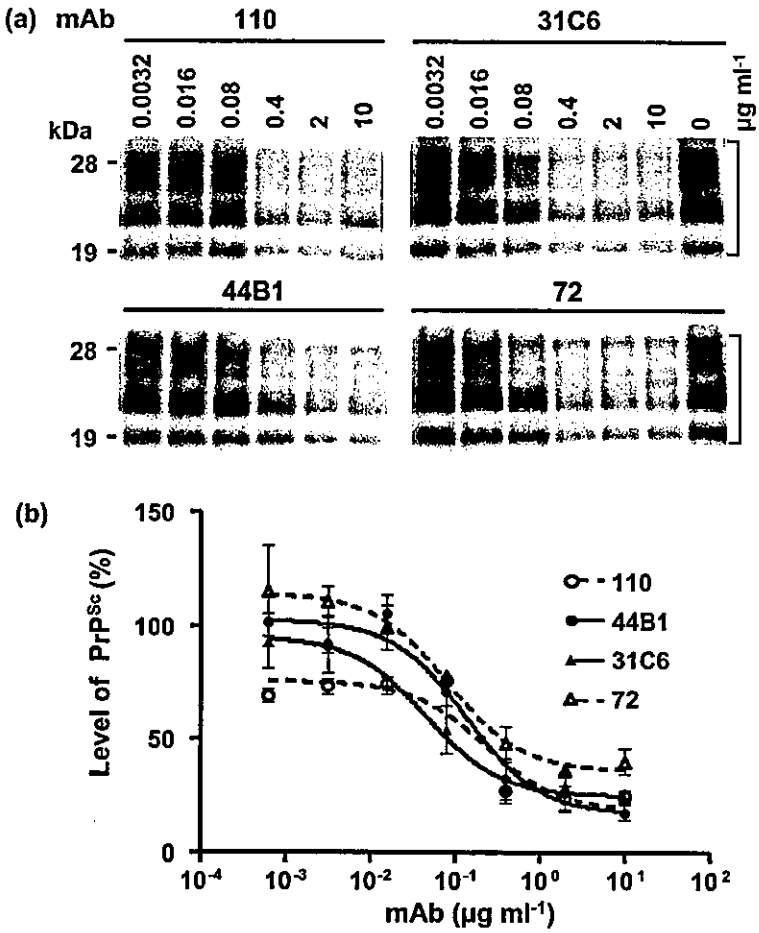

Fig. 2. Dose-dependent inhibition of PrP^{Sc} accumulation by anti-PrP mAbs. (a) Representative results from immunoblotting. I3/I5-9 cells were cultured for 3 days with various concentrations of mAb as indicated above the panels. The level of PrP^{Sc} was determined by immunoblot analysis using mAb 44B1. (b) Dose–response curve. The intensity of the PrP^{Sc} bands in the blots was quantified using an LAS-1000 lumino image analyser. The PrP^{Sc} level in the absence of mAbs was assigned a value of 100% in each experiment. The graph shows means ± SD from at least three independent experiments. EC_{50} values were estimated using GraphPad PRISM (GraphPad Software).

mAb–PrP^C complexes on the cell surface, we examined the effect of DS500, which is reported to accelerate PrP^C endocytosis (Shyng *et al.*, 1995). Following treatment with DS500, the mAb–PrP^C complexes on the cell surface were internalized and detected as intracellular granules (Fig. 5k–o). These results demonstrated that the mAbs bound to the cell-surface PrP^C remained there, regardless of their epitope specificity.

Effect of other compounds on PrP^C expression

Our results indicated a possible link between cell-surface retention of PrP^C by anti-PrP antibodies and the inhibition of PrP^{Sc} formation in cells, and suggested that the mAb treatment altered the total amount of PrP^C at least for mAbs 110 and 44B1. In order to examine whether compounds that inhibit PrP^{Sc} accumulation in prion-infected cells affect PrP^C level in the cells, we tested DS500, E-64d, quinacrine, chlorpromazine and polyethyleneimine. We confirmed that these compounds inhibited PrP^{Sc} accumulation in I3/I5-9 cells (data not shown). Using the concentrations at which these compounds caused >90% inhibition, we examined their effects on cellular levels of PrP^C following a 3-day treatment (Fig. 6a). Immunoblot analysis revealed that only DS500 reduced the PrP^C level (to ~30% that of untreated cells) among the compounds tested. Flow cytometric analysis with mAb 110 (Fig. 6b) confirmed that DS500 reduced the level of cell-surface PrP^C.

Since sulfated glycosaminoglycans like DS500 may bind to the N-terminal region of PrP^C (Pan *et al.*, 2002), the reduction in fluorescence intensity may be due to blocking of mAb 110 binding. For this reason, we used mAbs 31C6 and 44B1 to detect PrP^C instead of mAb 110. Table 1 shows the mean relative amount of PrP^C on the cell surface calculated from at least three independent experiments. Regardless of the mAb used for detection, DS500 reduced the PrP^C level to ~50% of the untreated control. No significant change in cell-surface expression of PrP^C was observed with the other compounds tested.

DISCUSSION

Anti-PrP antibodies that react with the C-terminal portion of PrP inhibit PrP^{Sc} formation in cultured cells (Enari *et al.*, 2001; Peretz *et al.*, 2001). One explanation for the inhibitory effect of these antibodies is that the binding of mAb to the corresponding epitope on PrP^C directly inhibits PrP^C–PrP^{Sc} interaction by occupying their binding domains. Fab D18, the most effective mAb reported by Peretz *et al.* (2001), reacts with the region spanning aa 132–156 in mouse PrP. In this study, we examined three mAbs

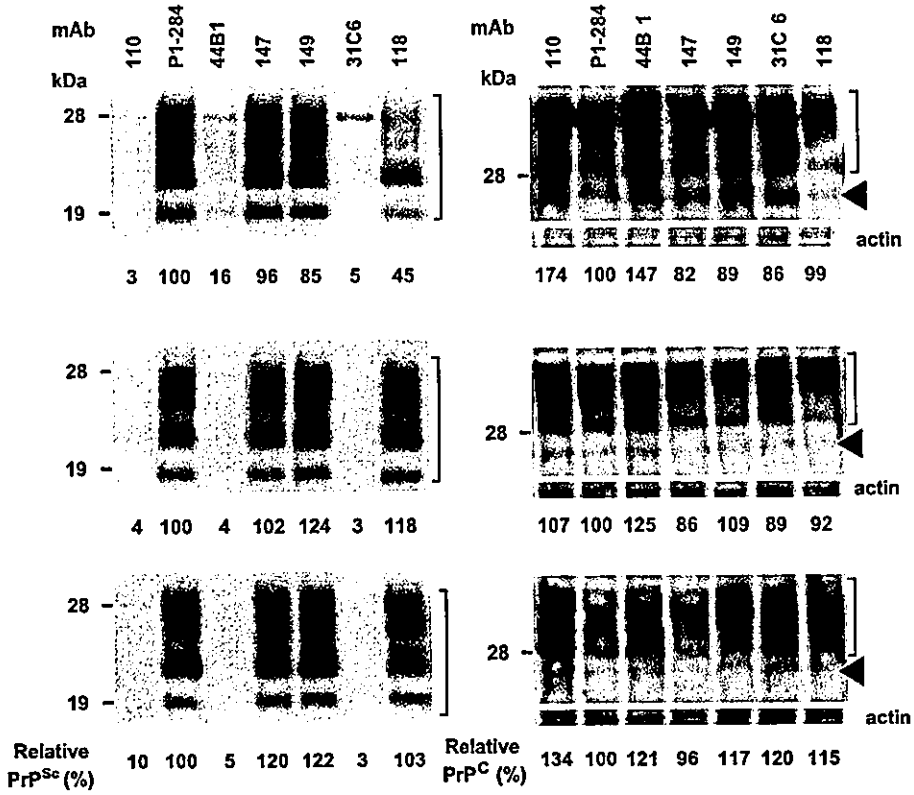

Fig. 3. Clearance of PrP^{Sc} by long-term antibody treatment. I3/I5-9 cells were cultured for 6 days with 5 μg mAb ml^{-1} (top panels). After withdrawal of the mAb, cells were cultured for an additional 6 (middle panels) or 12 (bottom panels) days in the absence of mAb. Quantitative analysis was carried out as described in the legend to Fig. 1 and relative PrP^{Sc} (left panels) and PrP^{C} (right panels) levels are indicated below the corresponding images.

recognizing epitopes within this region, but only mAb 31C6, which recognizes aa 143–149, displayed inhibitory activity. The remaining mAbs, 118 and 149, which bind adjacent epitopes aa 137–143 and aa 147–151, respectively, did not inhibit PrP^{Sc} formation in the cells. The main difference among these three mAbs was their ability to bind mature PrP^{C}; only mAb 31C6 bound PrP^{C} on the cell surface. Although it is well known that the N-terminal portion of PrP, including the octapeptide repeat, is not essential for prion propagation and/or PrP^{Sc} formation (Flechsig *et al.*, 2000; Rogers *et al.*, 1993), mAb 110, which recognizes the sequence in the octapeptide repeat, also antagonized PrP^{Sc} formation. This implied that there are mechanisms of inhibition other than blocking of the specific epitopes. Indeed, four of eight anti-PrP mAbs recognizing different epitopes inhibited PrP^{Sc} formation, suggesting that a common feature of the inhibitory mAbs is their ability to bind PrP^{C} on the cell surface. Taken together, our results suggest that inhibition of PrP^{Sc} formation by mAbs depends on their binding to mature PrP^{C} on the

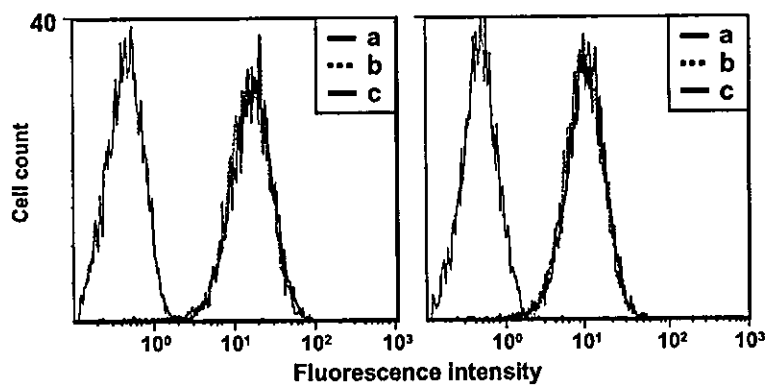

Fig. 4. Retention of mAb–PrP^{C} complexes on the cell surface. Neuro2a (left panel) or I3/I5-9 cells cured of PrP^{Sc} by mAb treatment (right panel) were cultured for 1 h in the presence of 10 μg negative control mAb P1-284 (a) or mAb 31C6 (b, c) ml^{-1}. Cells were harvested immediately and stained with Alexa-488-conjugated secondary antibody (a, b). Alternatively, after the removal of mAb, the cells were cultured for an additional 4 h in the absence of mAb and then harvested and stained with the secondary antibody (c).

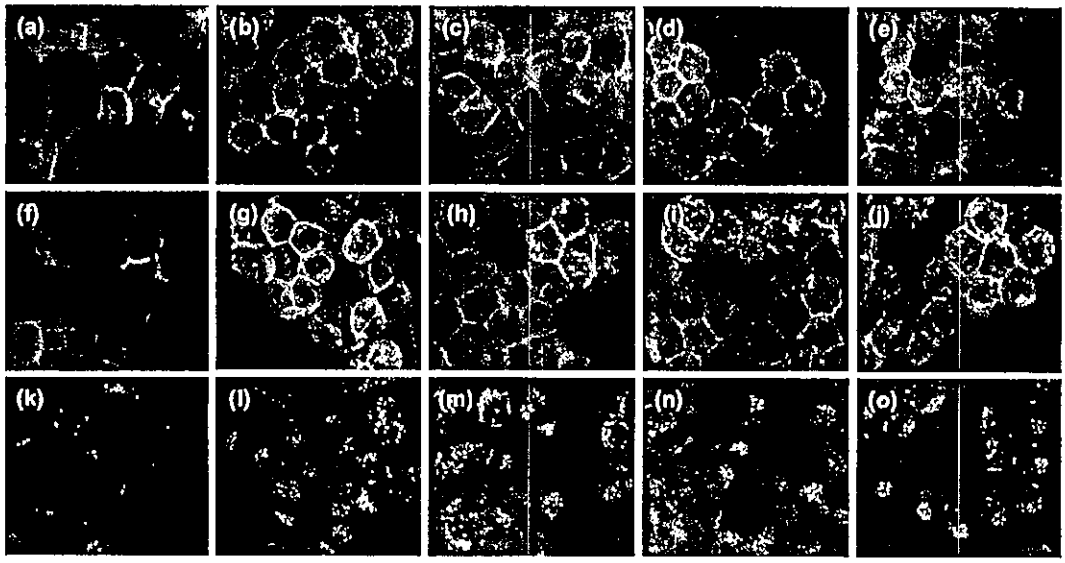

Fig. 5. Internalization of mAb–PrP^C complexes by treatment with DS500. Neuro2a cells (a, f and k) and I3/I5-9 cells (b–e, g–j, l–o) were cultured for 1 h with mAb 110 (b, g and l), 31C6 (a, f and k for Neuro2a cells; c, h and m for I3/I5-9 cells), 44B1 (d, i and n) or 72 (e, j and o). After removal of the mAb, cells were washed with ice-cold PBS and fixed with ice-cold methanol (a–e). Alternatively, after removal of mAb, cells were cultured with mAb-free medium for 4 h and fixed with ice-cold methanol (f–j). For DS500 treatment (k–o), after removal of mAb, cells were cultured for 3 h in mAb-free medium and then treated for 1 h with 25 μg DS500 ml^{-1}, after which they were fixed with ice-cold methanol. The fixed cells were directly stained with Alexa-488-conjugated secondary antibody to detect bound anti-PrP mAb.

cell surface rather than their binding to specific epitopes. On the other hand, transient interaction between the flexible N-terminal region and the second α-helix in the C-terminal globular domain has been postulated (Zahn *et al.*, 2000), and antibody binding to the N terminus of PrP prevents binding of C terminus-specific mAb (Li *et al.*, 2000). Hence, it cannot be excluded that binding of mAb 110 to the octapeptide repeat might sterically influence a particular domain involved in binding to PrP^{Sc}.

Although the cell-surface binding of mAb 110 was lower than that of the other mAbs (Fig. 1b, left panel), it inhibited PrP^{Sc} formation as efficiently. This may be explained by the presence of an 18 kDa N-terminally truncated PrP^C. This truncated PrP^C fragment is produced by cleavage of PrP^C around residue 112 during the recycling process (Chen *et al.*, 1995) so that it is not recognized by mAb 110. Recently, Mishra *et al.* (2002) reported that the N-terminally truncated form comprised as much as 40–50 % of PrP^C on the cell surface. This could account for the lower signals obtained using mAb 110. Because N-terminally truncated PrP^C is unlikely to act as a substrate for prion propagation and/or PrP^{Sc} formation (Lawson *et al.*, 2001; Weissmann, 1999), the binding of mAb 110 to PrP^C possessing the N-terminal portion is apparently sufficient for the inhibition of PrP^{Sc} formation.

In this work, we have demonstrated both quantitatively and qualitatively that mAbs that bind to cell-surface PrP^C remain attached to the membrane, even after withdrawal of the mAbs from the culture medium. This suggests that the mAb–PrP^C complex on the cell surface is not preferentially internalized into the cell. Mature PrP^C expressed on the cell surface is thought to be internalized via either clathrin-coated or -uncoated vesicles from which it enters the degradation pathway (Peters *et al.*, 2003; Shyng *et al.*, 1994; Sunyach *et al.*, 2003). Because PrP^{Sc} formation is believed to take place in the subcellular compartments that include cell membrane during the degradation pathway (Borchelt *et al.*, 1992; Caughey & Raymond, 1991), it is possible that mAb treatment could interfere with the regular PrP^C metabolism simply by retaining it on the cell surface. We suspected that the cell-surface retention of PrP^C would result in an increase in total PrP^C. Actually, two mAbs, 110 and 44B1, obviously increased the total amount of PrP^C, while two other mAbs 31C6 and 72 did not influence the total amount of PrP^C. It is conceivable that binding of mAbs to specific epitopes of cell-surface PrP^C might result in downregulation of PrP^C synthesis; however, further experiments are required to resolve this.

It was recently reported that polyclonal antibodies against dimeric recombinant PrP inhibited PrP^{Sc} formation in the cell, while the corresponding Fab fragments had little effect on PrP^{Sc} formation (Gilch *et al.*, 2003). This suggests that antibody-mediated cross-linking of PrP^C on the cell surface is important for inhibition of PrP^{Sc} formation. Whether cross-linking of PrP^C by IgG is required for the retention of the mAb–PrP^C complex under our experimental conditions remains to be determined. Treatment of cells persistently

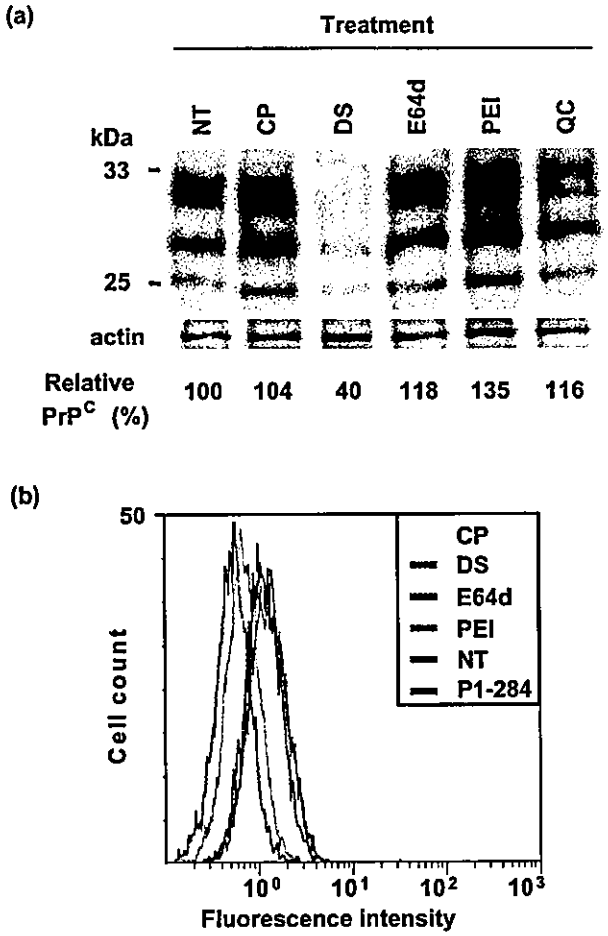

Fig. 6. Influence of chemical treatments on the expression of PrP^C. (a) Total amount of PrP^C. Neuro2a cells were treated for 12 h with various chemical compounds as indicated above the panel. Final concentrations were 3 μg chlorpromazine (CP) ml^{-1}, 25 μg DS500 (DS) ml^{-1}, 50 μM E-64d (E64d), 3 μg polyethyleneimine (PEI) ml^{-1} and 2 μM quinacrine (QC). Total PrP^C was detected in cell lysates by immunoblot analysis using mAb 31C6 (upper panel). The same blot was probed with anti-sarcomeric actin mAb to normalize for loading (lower panel). The intensity of the bands was quantified using an LAS-1000 lumino image analyser, and the relative amount of PrP^C compared with untreated control (NT) was calculated for each experiment. The data below the panel are means from three independent experiments. (b) Representative flow cytometric analysis of the cell-surface expression of PrP^C. Neuro2a cells were treated with compounds as described in (a), harvested, stained with mAb 110 followed by Alexa-488-conjugated secondary antibody and analysed by flow cytometry. The mean fluorescence intensity of the untreated control (NT) was assigned a value of 1 and the relative fluorescence intensities were calculated from the mean fluorescence intensity from each histogram. Quinarine was excluded from this experiment because of its autofluorescence. mAb P1-284 was used as a negative control for flow cytometric analysis.

Table 1. Effects of chemical treatment on cell-surface expression of PrP^C

Data represent means ± SD (minimum of $n=3$) of relative fluorescence intensity compared with control (NT).

Treatment	mAb for detection		
	110	31C6	44B1
NT	1·00	1·00	1·00
Chlorpromazine	0·77±0·05	0·95±0·03	0·92±0·03
DS500	0·52±0·03*	0·55±0·10*	0·48±0·04*
E-64d	0·99±0·17	0·99±0·06	0·97±0·11
Polyethyleneimine	1·01±0·16	1·04±0·03	1·07±0·11

*Statistically significant differences ($P<0·05$). The conditions of the treatments are described in the legend to Fig. 6.

infected with prions using antibodies against the laminin receptor precursor/laminin receptor (LRP/LR) reduced PrP^{Sc} accumulation (Leucht *et al.*, 2003). Because binding of LRP/LR to PrP^C could be involved in PrP metabolism (Gauczynski *et al.*, 2001), it is conceivable that antibodies interfere with the interaction between PrP^C and a molecule(s) that participates in PrP^C internalization.

Many reagents, including small molecules, recombinant PrP and anti-PrP antibodies, have been identified as potential inhibitors of prion propagation. It is important to elucidate their mechanisms of action, not only for the establishment of therapeutics but also for an understanding of prion replication. In the present study, we have demonstrated that blocking of the internalization of PrP^C with anti-PrP mAbs prevents PrP^{Sc} accumulation. Although anti-PrP mAbs recognizing specific epitopes have recently been reported to induce neuronal death in the hippocampus and cerebellum (Solforosi *et al.*, 2004), we have not found an apparent adverse effect on the cell growth and clinical manifestation by intraventricular inoculation of the anti-PrP mAbs used in this study (data not shown). Further analyses using prion-infected animals are necessary for evaluation of anti-PrP antibodies as therapeutics for treating prion diseases.

After the submission of this paper, a paper was published by Perrier *et al.* (2004) in which it was described that recognition by mAb SAF34 of the octapeptide repeat region on the N-terminal part of human PrP inhibited PrP^{Sc} formation in prion-infected neuroblastoma cells.

ACKNOWLEDGEMENTS

This work was supported by a grant from The 21st Century COE Program (A-1) and a Grant-in-Aid for Science Research (A) (grant 15208029) and (B) (grant 12460130) from the Ministry of Education, Culture, Sports, Science and Technology, Japan. This work was also supported by a grant from the Ministry of Health, Labour and Welfare of Japan.

REFERENCES

Borchelt, D. R., Taraboulos, A. & Prusiner, S. B. (1992). Evidence for synthesis of scrapie prion proteins in the endocytic pathway. *J Biol Chem* 267, 16188–16199.

Bueler, H., Aguzzi, A., Sailer, A., Greiner, R. A., Autenried, P., Aguet, M. & Weissmann, C. (1993). Mice devoid of PrP are resistant to scrapie. *Cell* 73, 1339–1347.

Caughey, B. & Race, R. E. (1992). Potent inhibition of scrapie-associated PrP accumulation by congo red. *J Neurochem* 59, 768–771.

Caughey, B. & Raymond, G. J. (1991). The scrapie-associated form of PrP is made from a cell surface precursor that is both protease- and phospholipase-sensitive. *J Biol Chem* 266, 18217–18223.

Caughey, B. & Raymond, G. J. (1993). Sulfated polyanion inhibition of scrapie-associated PrP accumulation in cultured cells. *J Virol* 67, 643–650.

Caughey, W. S., Raymond, L. D., Horiuchi, M. & Caughey, B. (1998). Inhibition of protease-resistant prion protein formation by porphyrins and phthalocyanines. *Proc Natl Acad Sci U S A* 95, 12117–12122.

Chabry, J., Caughey, B. & Chesebro, B. (1998). Specific inhibition of *in vitro* formation of protease-resistant prion protein by synthetic peptides. *J Biol Chem* 273, 13203–13207.

Chen, S. G., Teplow, D. B., Parchi, P., Teller, J. K., Gambetti, P. & Autilio-Gambetti, L. (1995). Truncated forms of the human prion protein in normal brain and in prion diseases. *J Biol Chem* 270, 19173–19180.

Demaimay, R., Adjou, K. T., Beringue, V., Demart, S., Lasmezas, C. I., Deslys, J. P., Seman, M. & Dormont, D. (1997). Late treatment with polyene antibiotics can prolong the survival time of scrapie-infected animals. *J Virol* 71, 9685–9689.

Demaimay, R., Race, R. & Chesebro, B. (1999). Effectiveness of polyene antibiotics in treatment of transmissible spongiform encephalopathy in transgenic mice expressing Syrian hamster PrP only in neurons. *J Virol* 73, 3511–3513.

Doh-Ura, K., Iwaki, T. & Caughey, B. (2000). Lysosomotropic agents and cysteine protease inhibitors inhibit scrapie-associated prion protein accumulation. *J Virol* 74, 4894–4897.

Doh-ura, K., Ishikawa, K., Murakami-Kubo, I., Sasaki, K., Mohri, S., Race, R. & Iwaki, T. (2004). Treatment of transmissible spongiform encephalopathy by intraventricular drug infusion in animal models. *J Virol* 78, 4999–5006.

Ehlers, B. & Diringer, H. (1984). Dextran sulphate 500 delays and prevents mouse scrapie by impairment of agent replication in spleen. *J Gen Virol* 65, 1325–1330.

Enari, M., Flechsig, E. & Weissmann, C. (2001). Scrapie prion protein accumulation by scrapie-infected neuroblastoma cells abrogated by exposure to a prion protein antibody. *Proc Natl Acad Sci U S A* 98, 9295–9299.

Flechsig, E., Shmerling, D., Hegyi, I., Raeber, A. J., Fischer, M., Cozzio, A., von Mering, C., Aguzzi, A. & Weissmann, C. (2000). Prion protein devoid of the octapeptide repeat region restores susceptibility to scrapie in PrP knockout mice. *Neuron* 27, 399–408.

Gauczynski, S., Peyrin, J. M., Haik, S. & 8 other authors (2001). The 37-kDa/67-kDa laminin receptor acts as the cell-surface receptor for the cellular prion protein. *EMBO J* 20, 5863–5875.

Gilch, S., Wopfner, F., Renner-Muller, I., Kremmer, E., Bauer, C., Wolf, E., Brem, G., Groschup, M. H. & Schatzl, H. M. (2003). Polyclonal anti-PrP auto-antibodies induced with dimeric PrP interfere efficiently with PrP^{Sc} propagation in prion-infected cells. *J Biol Chem* 278, 18524–18531.

Heppner, F. L., Prinz, M. & Aguzzi, A. (2001). Pathogenesis of prion diseases: possible implications of microglial cells. *Prog Brain Res* 132, 737–750.

Holscher, C., Delius, H. & Burkle, A. (1998). Overexpression of nonconvertible PrP^{c} Δ114–121 in scrapie-infected mouse neuroblastoma cells leads to *trans*-dominant inhibition of wild-type PrP^{Sc} accumulation. *J Virol* 72, 1153–1159.

Horiuchi, M. & Caughey, B. (1999). Specific binding of normal prion protein to the scrapie form via a localized domain initiates its conversion to the protease-resistant state. *EMBO J* 18, 3193–3203.

Horiuchi, M., Priola, S. A., Chabry, J. & Caughey, B. (2000). Interactions between heterologous forms of prion protein: binding, inhibition of conversion, and species barriers. *Proc Natl Acad Sci U S A* 97, 5836–5841.

Ishiyama, M., Tominaga, H., Shiga, M., Sasamoto, K., Ohkura, Y. & Ueno, K. (1996). A combined assay of cell viability and *in vitro* cytotoxicity with a highly water-soluble tetrazolium salt, neutral red and crystal violet. *Biol Pharm Bull* 19, 1518–1520.

Kaneko, K., Peretz, D., Pan, K. M. & 7 other authors (1995). Prion protein (PrP) synthetic peptides induce cellular PrP to acquire properties of the scrapie isoform. *Proc Natl Acad Sci U S A* 92, 11160–11164.

Kaneko, K., Zulianello, L., Scott, M., Cooper, C. M., Wallace, A. C., James, T. L., Cohen, F. E. & Prusiner, S. B. (1997). Evidence for protein X binding to a discontinuous epitope on the cellular prion protein during scrapie prion propagation. *Proc Natl Acad Sci U S A* 94, 10069–10074.

Kim, C.-L., Umetani, A., Matsui, T., Ishiguro, N., Shinagawa, M. & Horiuchi, M. (2004). Antigenic characterization of an abnormal isoform of prion protein using a new diverse panel of monoclonal antibodies. *Virology* 320, 40–51.

Korth, C., May, B. C., Cohen, F. E. & Prusiner, S. B. (2001). Acridine and phenothiazine derivatives as pharmacotherapeutics for prion disease. *Proc Natl Acad Sci U S A* 98, 9836–9841.

Ladogana, A., Casaccia, P., Ingrosso, L., Cibati, M., Salvatore, M., Xi, Y.-G., Masullo, C. & Pocchiari, M. (1992). Sulphate polyanions prolong the incubation period of scrapie-infected hamsters. *J Gen Virol* 73, 661–665.

Lawson, V. A., Priola, S. A., Wehrly, K. & Chesebro, B. (2001). N-terminal truncation of prion protein affects both formation and conformation of abnormal protease-resistant prion protein generated *in vitro*. *J Biol Chem* 276, 35265–35271.

Leucht, C., Simoneau, S., Rey, C., Vana, K., Rieger, R., Lasmezas, C. I. & Weiss, S. (2003). The 37 kDa/67 kDa laminin receptor is required for PrP^{Sc} propagation in scrapie-infected neuronal cells. *EMBO Rep* 4, 290–295.

Li, R., Liu, T., Wong, B.-S. & 7 other authors (2000). Identification of an epitope in the C terminus of normal prion protein whose expression is modulated by binding events in the N terminus. *J Mol Biol* 301, 567–573.

Mallucci, G., Dickinson, A., Linehan, J., Klohn, P. C., Brandner, S. & Collinge, J. (2003). Depleting neuronal PrP in prion infection prevents disease and reverses spongiosis. *Science* 302, 871–874.

Mishra, R. S., Gu, Y., Bose, S., Verghese, S., Kalepu, S. & Singh, N. (2002). Cell surface accumulation of a truncated transmembrane prion protein in Gerstmann–Straussler–Scheinker disease P102L. *J Biol Chem* 277, 24554–24561.

Murakami-Kubo, I., Doh-Ura, K., Ishikawa, K., Kawatake, S., Sasaki, K., Kira, J., Ohta, S. & Iwaki, T. (2004). Quinoline derivatives are therapeutic candidates for transmissible spongiform encephalopathies. *J Virol* 78, 1281–1288.

Naslavsky, N., Stein, R., Yanai, A., Friedlander, G. & Taraboulos, A. (1997). Characterization of detergent-insoluble complexes containing the cellular prion protein and its scrapie isoform. *J Biol Chem* **272**, 6324–6331.

Pan, T., Wong, B. S., Liu, T., Li, R., Petersen, R. B. & Sy, M. S. (2002). Cell-surface prion protein interacts with glycosaminoglycans. *Biochem J* **368**, 81–90.

Peretz, D., Williamson, R. A., Kaneko, K. & 10 other authors (2001). Antibodies inhibit prion propagation and clear cell cultures of prion infectivity. *Nature* **412**, 739–743.

Perrier, V., Solassol, J., Crozet, C., Frobert, Y., Mourton-Gilles, C., Grassi, J. & Lehmann, S. (2004). Anti-PrP antibodies block PrP^{Sc} replication in prion-infected cell cultures by accelerating PrP^{C} degradation. *J Neurochem* **89**, 454–463.

Peters, P. J., Mironov, A., Jr, Peretz, D. & 8 other authors (2003). Trafficking of prion proteins through a caveolae-mediated endosomal pathway. *J Cell Biol* **162**, 703–717.

Priola, S. A., Raines, A. & Caughey, W. S. (2000). Porphyrin and phthalocyanine antiscrapie compounds. *Science* **287**, 1503–1506.

Race, R. E., Fadness, L. H. & Chesebro, B. (1987). Characterization of scrapie infection in mouse neuroblastoma cells. *J Gen Virol* **68**, 1391–1399.

Rogers, M., Yehiely, F., Scott, M. & Prusiner, S. B. (1993). Conversion of truncated and elongated prion proteins into the scrapie isoform in cultured cells. *Proc Natl Acad Sci U S A* **90**, 3182–3186.

Shyng, S. L., Heuser, J. E. & Harris, D. A. (1994). A glycolipid-anchored prion protein is endocytosed via clathrin-coated pits. *J Cell Biol* **125**, 1239–1250.

Shyng, S. L., Lehmann, S., Moulder, K. L. & Harris, D. A. (1995). Sulfated glycans stimulate endocytosis of the cellular isoform of the prion protein, PrP^{C}, in cultured cells. *J Biol Chem* **270**, 30221–30229.

Sigurdsson, E. M., Brown, D. R., Daniels, M., Kascsak, R. J., Kascsak, R., Carp, R., Meeker, H. C., Frangione, B. & Wisniewski, T. (2002). Immunization delays the onset of prion disease in mice. *Am J Pathol* **161**, 13–17.

Solforosi, L., Criado, J. R., McGavern, D. B. & 12 other authors (2004). Cross-linking cellular prion protein triggers neuronal apoptosis *in vivo*. *Science* **303**, 1514–1516.

Soto, C., Kascsak, R. J., Saborio, G. P. & 10 other authors (2000). Reversion of prion protein conformational changes by synthetic β-sheet breaker peptides. *Lancet* **355**, 192–197.

Sunyach, C., Jen, A., Deng, J., Fitzgerald, K. T., Frobert, Y., Grassi, J., McCaffrey, M. W. & Morris, R. (2003). The mechanism of internalization of glycosylphosphatidylinositol-anchored prion protein. *EMBO J* **22**, 3591–3601.

Supattapone, S., Nguyen, H.-O. B., Cohen, F. E., Prusiner, S. B. & Scott, M. R. (1999). Elimination of prions by branched polyamines and implications for therapeutics. *Proc Natl Acad Sci U S A* **96**, 14529–14534.

Supattapone, S., Wille, H., Uyechi, L., Safar, J., Tremblay, P., Szoka, F. C., Cohen, F. E., Prusiner, S. B. & Scott, M. R. (2001). Branched polyamines cure prion-infected neuroblastoma cells. *J Virol* **75**, 3453–3461.

Vey, M., Pilkuhn, S., Wille, H., Nixon, R., DeArmond, S. J., Smart, E. J., Anderson, R. G., Taraboulos, A. & Prusiner, S. B. (1996). Subcellular colocalization of the cellular and scrapie prion proteins in caveolae-like membranous domains. *Proc Natl Acad Sci U S A* **93**, 14945–14949.

Weissmann, C. (1999). Molecular genetics of transmissible spongiform encephalopathies. *J Biol Chem* **274**, 3–6.

White, A. R., Enever, P., Tayebi, M., Mushens, R., Linehan, J., Brandner, S., Anstee, D., Collinge, J. & Hawke, S. (2003). Monoclonal antibodies inhibit prion replication and delay the development of prion disease. *Nature* **422**, 80–83.

Xi, Y.-G., Ingrosso, L., Ladogana, A., Masullo, C. & Pocchiari, M. (1992). Amphotericin B treatment dissociates *in vivo* replication of the scrapie agent from PrP accumulation. *Nature* **356**, 598–601.

Zahn, R., Liu, A., Lührs, T. & 7 other authors (2000). NMR solution structure of the human prion protein. *Proc Natl Acad Sci U S A* **97**, 145–150.

NOTE *Clinical Pathology*

Unique Amino Acid Polymorphisms of PrP Genes in Mongolian Sheep Breeds

Altangerel GOMBOJAV[1,3], Naotaka ISHIGURO[1]*, Motohiro HORIUCHI[1] and Morikazu SHINAGAWA[2]

[1]*Laboratory of Veterinary Public Health, Obihiro University of Agriculture and Veterinary Medicine, Obihiro, Hokkaido 080–8555,*
[2]*Prion Disease Research Center, National Institute of Animal Health, 5–1–3 Kannondai, Tsukuba, Ibaraki 305–0856, Japan and*
[3]*School of Veterinary Medicine and Biotechnology, Mongolian State University of Agriculture, Ulaanbaatar 210153, Zaisan, Mongolia*

(Received 1 August 2003/Accepted 27 May 2004)

ABSTRACT. To characterize amino acid polymorphisms of sheep prion protein (PrP) gene, DNA from 740 sheep of nine breeds raised in Mongolia was isolated and analyzed. A total of 16 genotypes and seven allelic variants of the PrP gene at codons 112, 136, 154, and 171 were found. The MARQ/MARQ genotype associated with susceptibility to scrapie was found in 82.6% of the sheep while the MARR/MARR genotype associated with resistance to scrapie was found in 1.8% of the sheep. The polymorphisms of valine and serine at codon 127, and leucine and arginine at codon 189 were detected in eight Mongolian sheep breeds, suggesting that these polymorphisms are a common feature among Mongolian sheep breeds.
KEY WORDS: PrP genotype, scrapie susceptibility.

J. Vet. Med. Sci. 66(10): 1293–1295, 2004

Scrapie in sheep and goats is a fatal and infectious neurodegenerative disease that has been categorized as a transmissible spongiform encephalopathy (TSE) or prion disease also found in humans and other animals. Prion diseases are characterized by the accumulation in the tissues of the central nervous system of an "infectious" abnormal protease-resistant isoform (PrP^{Sc}) of cellular prion proteins (PrP^{C}) encoded by the PrP gene [12]. Polymorphisms of the PrP gene have been linked to host susceptibility and the incubation period of the disease [11]. PrP allelic variant valine/arginine/glutamine (VRQ) at codons 136, 154, and 171 is associated with high susceptibility to scrapie for sheep breeds. While the allele VRQ is rare in Suffolk sheep, the wild-type PrP allele alanine/arginine/glutamine (ARQ) is associated with susceptibility to scrapie. It has been widely considered that the PrP allelic variant alanine/arginine/arginine (ARR) at codons 136, 154, and 171 is associated with resistance to scrapie in several breeds [1–5, 7–10, 13]. Links between DNA polymorpisms and scrapie susceptibility have been identified in outbreaks of scrapie in various breeds or flocks in different countries where scrapie has been diagnosed [1, 7–8, 10, 13]. However, in central Asian countries where many sheep are raised, the polymorpism of PrP genes associated with scrapie have not yet been characterized. Therefore, we examined the PrP genotypes of 740 Mongolian sheep, including 271 sheep previously reported [6].

DNA samples were collected from several breeds from different prefectures in Mongolia. A total of 271 sheep came from the central region of Mongolia: 112 Khalkh sheep (native breed) from Tuv prefecture (designated I in Fig. 1.); 60 Khalkh sheep from Uvurkhangai prefecture (J); and 35 Yeroo sheep, 35 Orkhon sheep, and 29 Khangai sheep from Selenge prefecture (K) [6]. From the western region, a total of 345 sheep were used: 70 Khalkh sheep and 36 Sartuul sheep from Zavhan prefecture (A); 35 Khalkh sheep and 35 Govi-altai sheep from Govi-Altai prefecture (B); 71 Khalkh sheep and 33 Bayad sheep from Uvs prefecture (C); and 34 Khalkh sheep and 31 Darhad sheep from Huvsgul prefecture (D). For the eastern region, a total of 124 sheep were used: 32 Sumber Karakul sheep from Govi-Sumber prefecture (H); 32 Khalkh sheep from Dornogovi prefecture (E); 31 Khalkh sheep from Suhbaatar prefecture (F); and 29 Khalkh sheep from Hentii prefecture (G). The Khalkh sheep comprised about 90% of 13.8 million Mongolian sheep. Crossbreeding between the Khalkh sheep and local sheep including imported sheep started in the 1930s, and the crossbreeding has led to develop several local crossbreeds in Mongolia [6].

The entire 794-bp open reading frame (ORF) of the PrP gene was amplified by polymerase chain reaction (PCR) in 50 μl reactions, using PrP primers (SPrP-1, SPrP-2, SPrP-3, and SPrP-5) as described by Gombojav *et al.* [6]. To confirm amplification, a portion of each reaction product was electrophoresed on a 0.7% agarose gel containing ethidium bromide (0.5 $\mu g/ml$), and visualized under ultraviolet radiation. Then, the primers were removed using a Centricon 100 micro-concentrator (Amicon, Bedford, MA), and 1 to 5 μl of the concentrated PCR product was used for direct sequencing [6].

In this study, the relative genotype frequencies of four codons (112, 136, 154, and 171) of the PrP gene are newly reported in five sheep breeds (Sartuul, Govi-altai, Bayad, Darhad, and Sumber Karakul), in addition to four previously reported sheep breeds (Khalkh, Yeroo, Orkhon, and Khangai) [6]. Table 1 shows the genotype frequencies of 16 different PrP genotypes in the 740 sheep examined. The PrP genotypes MARQ/MARQ was found in all nine breeds.

Among all the breeds studied, the Khalkh sheep showed the greatest variation with 11 PrP genotypes composed from 6 alleles, while three to nine PrP genotypes were found in

* CORRESPONDENCE TO: ISHIGURO, N., Laboratory of Veterinary Public Health, Obihiro University of Agriculture and Veterinary Medicine, Obihiro, Hokkaido 080–8555, Japan.

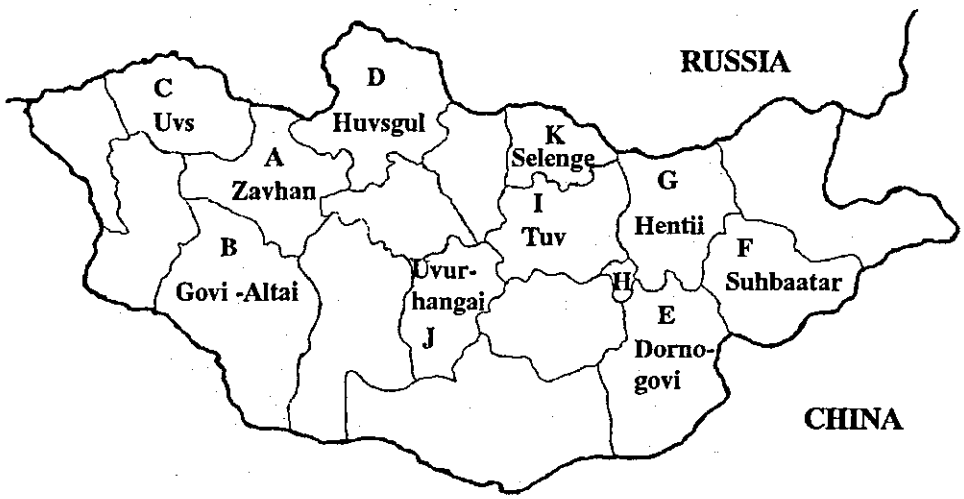

Fig. 1. Map of Mongolia. The blood samples were collected from different prefectures in Mongolia (A-K). H, Govi-Sumber prefecture.

Table 1. Frequency of PrP genotypes at codons 112, 136, 154 and 171 in Mongolian sheep breeds

Location[a]	A-G, I-J		A		B		C		D		H		K		K		K	
Breeds	Khalkh[b]		Sartuul		Govi-altai		Bayad		Darhad		Sumber		Yeroo[c]		Orkhon[c]		Khangai[c]	
PrP genotype											Karakul							
	No	%	No	%	No	%	No	%	No	%	No	%	No	%	No	%	No	%
MARQ/MARQ	317	66.8	29	80.6	27	77.1	29	87.9	21	67.7	27	84.3	17	48.5	13	37.0	15	51.7
MARQ/TARQ	68	14.4	3	8.3	2	5.7	3	9.1	2	6.5			4	11.4	7	20.0	2	6.9
MARQ/MARH	31	6.6	2	5.5	2	5.7	1	3.0	5	16.2	3	9.4			1	2.9		
MARQ/MARR	13	2.7			2	5.7							8	22.8	8	22.8	9	31.0
MARH/MARH	7	1.5	1	2.8					1	3.2	2	6.3			1	2.9		
TARQ/TARQ	12	2.5							1	3.2			1	2.9				
TARQ/MARH	8	1.7													1	2.9		
TARQ/MARR	4	0.8			1	2.9									1	2.9		
MARQ/MAHQ	6	1.3																
MARR/MARR	7	1.5			1	2.9			1	3.2			2	5.7			2	6.9
MARK/MARK	1	0.2	1	2.8														
MARQ/MVRQ													1	2.9	2	5.7		
MARR/MVRQ													1	2.9				
MARH/MAHQ													1	2.9				
MARR/MAHQ															1	2.9		
TARQ/MAHQ																	1	3.5
Total	474		36		35		33		31		32		35		35		29	

a) Locations are shown in Fig. 1.
b) A total of 474 samples include 172 samples previously reported by Gombojav *et al.* [6].
c) Data from Gombojav *et al.* [6].

the other sheep breeds. The great variations in PrP genotypes suggest that Khalkh sheep originated from a mixture of several breeds from surrounding countries, while lesser variations in the other sheep breeds suggest that these breeds originated from a mixture of fewer numbers of breeds within Mongolia.

The allelic variant VRQ at codons 136, 154, and 171 is rare in Suffolk sheep [4, 9, 13] and this tendency was also found in the Mongolian sheep breeds. Valine at codon 136 (136V) associated with high susceptibility to scrapie was detected from two sheep breeds, Yeroo and Orkhon, but not in the other sheep breeds of Mongolia. Yeroo and Orkhon sheep have been raised in Selenge prefecture, which is in close proximity to Russia. The sheep raised in the prefecture had been genetically developed by crossbreeding with Russian sheep. Therefore, it is thought that the polymorphism of valine at codon 136 may have been introduced through the Russian sheep breeds, although little information about the PrP polymorphism of Russian sheep.

We found valine (V; nucleotides GTC) and serine (S;

Table 2. Frequency of PrP genotypes at codons 127 and 189 in Mongolian sheep breeds

Location[a]	A-G, I-J		A		B		C		D		H		K		K		K	
Breeds	Khalkh[b]		Sartuul		Govi-altai		Bayad		Darhad		Sumber		Yeroo[c]		Orkhon[c]		Khangai[c]	
PrP genotype	No	%	No	%	No	%	No	%	No	%	Karakul No	%	No	%	No	%	No	%
GQ/GQ[d]	354	74.6	26	72.2	17	48.6	22	66.8	20	64.5	23	71.9	28	80.0	32	91.4	29	100
GQ/SQ	68	14.4	5	13.9	4	11.4	6	18.2	8	25.8	5	15.6	7	20.0	1	2.9		
SQ/SQ	5	1.1									1	3.1						
GQ/VQ	19	4.0					1	3.0			2	6.3						
GQ/GL	20	4.2	4	11.1	11	31.4	2	6.0	3	9.7	1	3.1			2	5.7		
GL/GL	1	0.2																
GQ/GR	2	0.4			1	2.9												
GL/SQ	5	1.1	1	2.8	2	5.7	2	6.0										
Total	474		36		35		33		31		32		35		35		29	

a) Locations are shown in Fig. 1.
b) A total of 474 samples include 172 samples previously reported by Gombojav *et al.* [6]
c) Data from Gombojav *et al.* [6].
d)Wild type of sheep PrP gene.

AGC) at codon 127, and leucine (L; CTA) and arginine (R; CGA) at codon 189 in eight Mongolian sheep breeds (Table 2). These amino acid polymorphisms of PrP gene were widely observed in Mongolian sheep breeds but have not been reported in other sheep from European countries, suggesting that these are unique to indigenous sheep breeds including Mongolian sheep. However, it remains to be determined whether these polymorphisms have any correlation with susceptibility to scrapie.

Among the different sheep breeds raised in Mongolia, 66.9% had the MARQ/MARQ genotype and 1.8% had the MARR/MARR genotype, which are linked to susceptibility and resistance to scrapie, respectively (Table 1). In the previous study [6], we examined the scrapie form of the prion protein (PrP^{Sc}) in brain tissues from 10 sheep with neurological symptoms, but no PrP^{Sc} was obtained by Western blot analysis. Therefore, although there have been no reports of scrapie in Mongolia, these results suggest that the majority of Mongolian sheep are genetically susceptible to scrapie. However, since PrP genes linked to scrapie resistance were observed in five of the nine breeds, individual sheep carrying the scrapie-resistant genes can be identified and used in breeding programs to develop scrapie-resistant populations.

ACKNOWLEDGEMENTS. This work was partly supported by a grant from the Ministry of Health and Welfare of Japan, from Ministry of Agriculture, Forestry and Fisheries of Japan and Grant-in-Aid for Science Research from the Ministry of Education, Science and Culture of Japan (12460130, 12575030, 10556069).

REFERENCES

1. Belt, P.B.G.M., Muileman, I.H., Schreuder, B.E.C., Bos-de Ruijter, J., Gielkens, A.L.J. and Smits, M.A. 1995. *J. Gen. Virol.* **76**: 509–517.
2. Bossers, A., Screuder, B.E.C., Muileman, I.H., Belt, P.B.G.M. and Smits, M.A. 1996. *J. Gen. Virol.* **77**: 2669–2673.
3. Clouscard, C., Beaudry, P., Elsen, J.M., Milan, D., Dussaucy, M., Bounneau, C., Schelcher C.J., Launay, J.M. and Laplanche, J.L. 1995. *J. Gen. Virol.* **76**: 2097–2101.
4. Goldmann, W., Hunter, N., Foster, J.D., Salbaum, J.M., Beyreuther, K. and Hope, J. 1990. *Proc. Natl. Acad. Sci. U.S.A.* **87**: 2476–2480.
5. Goldmann, W., Hunter, N., Smith, G., Foster, J.D. and Hope, J. 1994. *J. Gen. Virol.* **75**: 989–995.
6. Gombojav, A., Ishiguro, N., Horiuchi, M., Serjmyadag, D., Byambaa, B. and Shinagawa, M. 2003. *J. Vet. Med. Sci.* **65**: 78–81.
7. Hunter, N., Foster, J.D., Goldmann, W., Stear, M.J., Hope, J. and Bostock, C. 1996. *Arch. Virol.* **141**: 809–824.
8. Hunter, N., Goldmann, W., Benson, G., Foster, J.D. and Hope, J. 1993. *J. Gen. Virol.* **74**: 1025–1031.
9. Hunter, N., Goldmann, W., Smith, G. and Hope, J. 1994. *Arch. Virol.* **137**: 171–177.
10. Laplanche, J.L., Chatelain, J., Westaway, D., Thomas, S., Dussaucy, M., Brugere-Picoux, J. and Launay, J.M. 1993. *Genomics* **15**: 30–37.
11. Loftus, B., Monks, E., Hanlon, J., Weavers, E. and Rogers, M. 1999. *Ir. Vet. J.* **52**: 81–85.
12. Prusiner, S.B. 1991. *Science* **252**: 1515–1522.
13. Westaway, D., Zuliani, V., Mirenda C.C., Da Costa, M., Neuman, S., Jenny, A.L., Detwiler, L. and Prusiner, S.B. 1994. *Genes. Dev.* **8**: 959–969.

Articles

Slow Conformational Dynamics in the Hamster Prion Protein†

Kazuo Kuwata,*,# Yuji O. Kamatari,⊥ Kazuyuki Akasaka,‡ and Thomas L. James*,§

Department of Biochemistry and Biophysics, School of Medicine, Gifu University, Gifu 500-8705 Japan, Cellular Signaling Laboratory, RIKEN Harima Institute, Hyogo, 679-5148 Japan, Department of Biotechnological Sciences, School of Biology-Oriented Science and Technology, Kinki University, Wakayama, 649-6493 Japan, and Department of Pharmaceutical Chemistry, 600 16th Street, Genentech Hall, University of California, San Francisco, California, 94143-2280 USA

Received November 25, 2003; Revised Manuscript Received February 9, 2004

ABSTRACT: Although the mechanism of the conformational conversion from the cellular (PrP^C) to the scrapie (PrP^{Sc}) form of animal prion proteins has yet to be elucidated, evidence is accumulating that may provide insight into the conversion process at atomic resolution. Here we show critical aspects of the slow fluctuation dynamics of the recombinant hamster prion protein, rPrP(90−231), based on NMR relaxation analysis using Carr-Purcell-Meiboom-Gill (CPMG) experiments, and compare them in detail with results from high-pressure NMR. Residues exhibiting slow fluctuations on the time scale of microseconds to milliseconds are mainly localized on helices B and C (172−193 and 200−227), which include locally disordered regions in an intermediate conformer, PrP*, identified previously by high-pressure NMR [Kuwata, K., et al., (2002) *Biochemistry* 41, 12277−12283]. Moreover, chemical shift differences between two putative exchanging conformers obtained by the CPMG relaxation analysis and the linear component of the pressure-induced chemical shift changes are reasonably correlated at individual residue sites. These observations suggest that both the CMPG relaxation and the pressure shifts reflect slow conformational fluctuations and that these slow motions in PrP^C are related to the trajectories leading to the transition to PrP*.

Prions cause neurodegenerative diseases, such as scrapie in sheep, bovine spongiformencephalopathy (BSE) in cattle, Creutzfeldt-Jakob disease (CJD), Gerstmann-Sträussler-Scheinker syndrome (GSS), fatal familial insomnia (FFI), kuru, and a new variant of CJD in humans (*1*−*3*). These diseases are associated with conversion of the normal cellular form of the prion protein (PrP^C) to a pathogenic scrapie form (PrP^{Sc}), which is apparently the infectious agent in transmitted forms of the disease (*3*, *4*). The sequences of PrP^{Sc} and the noninfectious precursor PrP^C are identical (*5*). Although both isoforms are chemically identical, they possess very different physicochemical properties. PrP^C is substantially helical, but PrP^{Sc} has ~40% β-sheet (*6*).

The three-dimensional structure of PrP^C was first elucidated for the mouse, Mo PrP (121−231) (*7*), and the hamster species, SHa PrP (90−231) (*8*), by NMR. Subsequently, structures for bovine (*9*) and human (*10*) species were elucidated. While there are some species-specific differences, the structures are similar in that residues 128−231 constitute a globular fold with three α-helices, a small, imperfectly formed and conformationally flexible β-sheet composed of antiparallel strands S1 and S2, an N-terminal segment up to residue 113 completely disordered and, at least in the hamster species, a hydrophobic cluster (residues 113−128) with multiple interconverting conformers (*11*).

NMR studies of dynamics in the PrP^C structure were reported (*11*, *12*) using heteronuclear NOE, T_1, T_2, and off-resonance $T_{1\rho}$ relaxation time measurements (*12*). The results are consistent with the static picture of PrP^C, i.e., the central portions of helices B and C form a relatively rigid core, but the remainder of the globular domain and helix A are more flexible on a picosecond-to-nanosecond time scale. Slow conformational fluctuations on the microsecond-to-millisecond time scale were observed only for the small β-sheet and the hydrophobic cluster (*11*, *12*).

However, our recent results for conformational fluctuations by high-pressure NMR were quite different from that static picture, possibly due to the difference in the time scale of the fluctuations (*13*). Consequently, here we examined NMR relaxation results for SHa PrP (90−231) using the Carr-Purcell-Meiboom-Gill (CPMG) method (*14*) as well as standard T_1, T_2, and NOE measurements, together with a

† Supported in part by Grants-in-Aid for Scientific Research from the Ministry of Education, Culture, Sports, Science and Technology of Japan (14380314, 14037224) and by the Gifu Prefecture Brain Research Foundation.

* To whom correspondence should be addressed. E-mail: james@picasso.ucsf.edu; tel.: (415) 476-1916; fax: (415) 502-8298 or e-mail: kuwata@cc.gifu-u.ac.jp; tel: +81-582-67-2227; fax: +81-582-67-2962.

Gifu University.

⊥ RIKEN Harima Institute.

‡ Kinki University.

§ University of California.

10.1021/bi036123o CCC: $27.50
Published on Web 03/26/2004

further detailed analysis of the high-pressure NMR results. All of these data pertaining to prion protein dynamics are examined in the context of biological and clinical observations (*15*).

MATERIALS AND METHODS

Samples. Expression, isotopic labeling, purification, and considerations for proper refolding of recombinant Syrian hamster prion protein rPrP (90−231) have been described previously (*11*, *13*). Purified rPrP (90−231), labeled uniformly with ^{15}N, was lyophilized before refolding. Samples were analyzed by mass spectroscopy, circular dichroism, and Fourier transform infrared spectroscopy to ensure the refolded rPrP (90−231) resembles PrP^C, i.e., is largely α-helical.

NMR Measurements. The online high-pressure NMR system contains the protein solution in a quartz tube cell that endures pressures of ≥2500 bar. The cell was connected to a high-pressure line via frictionless Teflon pistons that separate the protein solution from the pressure mediator (kerosene) in a separator cylinder (BeCu). The cell body (inner diameter 1 mm, outer diameter 3 mm) is positioned in a commercial 5-mm NMR probe (Bruker). Pressure was regulated to a desired value between 1 and 2500 bar with a remote hand-pump and maintained at that value during signal accumulation. For 1D and 2D NMR measurements, samples were dissolved in 95% ^1H_2O/5% ^2H_2O containing 20 mM sodium acetate, pH 5.2, to make a 1 mM protein solution. As chemical shift references, trace amounts of sodium 3-trimethylsilyl-(2,2,3,3-^2H)-tetradeuteriopropionate (TSP-d_4) and dioxane were added to the solution. The dioxane resonance remains unchanged with pressure (3.750 ppm from TSP at 1 bar). Relaxation time measurements were performed in standard Shigemi tubes with 11.7 T (Varian Inova 500) and 18.8 T NMR spectrometers (Bruker Avance 800).

Reduced Spectral Density Mapping. ^{15}N longitudinal (T_1) and transverse (T_2) relaxation times and {^1H}-^{15}N heteronuclear NOEs were measured using two different magnetic fields, 11.7 T (500 MHz proton frequency) and 18.8 T (800 MHz). Several peaks are overlapped and are not presented here. For residues 100−231, the R_1 (=$1/T_1$) rates are relatively invariant around 1.5 s^{-1} at 11.7 T. At 18.8 T, for residues 128−231, they are all approximately 1.0 s^{-1}. For residues 100−110, R_1 values are about 1.5 s^{-1}, indicating the relative invariance to the magnetic field strength, which is commonly observed for natively unfolded protein (*16*, *17*). The reduced spectral density function, $J(\omega)$, provides insights into the motion of the N−H bond vector at five frequencies: 0, ω_{N1} (0.32 gigaradian (grad)/s), ω_{N2} (0.51 grad/s), $0.87\omega_{H1}$ (2.73 grad/s), and $0.87\omega_{H2}$ (4.37 grad/s), where 1 and 2 denote angular velocities at 11.7 and 18.8 T, respectively. The largest value of $J(0)$ is ~6 ns at 11.7 T and ~5 ns at 18.8 T. The different $J(0)$ values at 11.7 and 18.8 T demonstrate the inherent limitation of deriving absolute $J(0)$ values from first-order reduced spectral density mapping. The $J(0)$ values at 11.8 T are used in Figure 6a (vide infra).

Slow Fluctuation Analysis. Values of the exchange lifetime τ_{ex} were calculated from the dependence of the signal intensities on interpulse spacing in the CPMG experiment (*13*, *14*). The pulse sequence for measuring the ^{15}N R_2 values (*18*−*20*) was used with modifications for averaging in-phase and antiphase coherence (*21*, *22*).

The apparent transverse relaxation rate with two-site chemical exchange can be expressed as (*14*)

$$R_2^* = R_2 + \tau_{ex} f_1 f_2 (\Delta\omega)^2 \left[1 - \frac{2\tau_{ex}}{\tau_{cp}} \tanh\left(\frac{\tau_{cp}}{2\tau_{ex}}\right)\right] \quad (1)$$

where τ_{cp} is the delay between 180° pulses in the CPMG sequence, and $\Delta\omega$ is the difference in chemical shift of the nucleus in the two conformational states. τ_{ex} (= $\tau_{-1} f_1 = \tau_1 f_2$) is the exchange time constant. f_1 and f_2 (= $1 - f_1$) are the fractions of populations of the two conformational states, and τ_1 and τ_{-1} are forward and the reverse exchange time constants, respectively. R_2 is the pure transverse relaxation rate due to the molecular motion on the time scale of picoseconds to nanoseconds without the slow exchange contribution on the microsecond-to-millisecond time scale. Numerical calculation using the exact equation (*23*) shows that eq 1 is accurate within 5% when $\Delta\omega < 4$ ppm and $\tau_{cp}/\tau_{ex} < 10^{-2}$. In our case, $(f_1 f_2)^{1/2}\Delta\omega \sim 0.1$ kHz, and $\tau_{ex} \sim 0.002$ s. However, since the exact equation is still a monotonic function of $\Delta\omega$ and τ_{ex}, we may be able to characterize these parameters qualitatively rather than quantitatively, even when $(f_1 f_2)^{1/2}\Delta\omega > 0.1$ kHz, and $\tau_{ex} > 0.002$ s. This is illustrated by representative examples of nonlinear fits that are shown in Supporting Information.

High-Pressure NMR Analysis. In general, the conformation of a protein molecule in solution may consist of an equilibrium mixture of conformers differing in topology of folding (e.g., between the native conformer N and an intermediate partially folded conformer I), in partial molar volume V, as well as in thermodynamic stability ΔG. In this situation, the equilibrium constant K between N and I may change with pressure according to the relation:

$$K = [\mathrm{I}]/[\mathrm{N}] = \exp(-\Delta G/RT) \quad (2)$$

where

$$\Delta G = G(\mathrm{I}) - G(\mathrm{N}) = \Delta G_0 + \Delta V(p - p_0) - (1/2)\Delta\beta V (p - p_0)^2 \quad (3)$$

ΔG and ΔG_0 are the Gibbs free energy changes from N to I at pressure p and p_0 (= 1 bar), respectively, ΔV is the partial molar volume change, $\Delta\beta$ is the change in compressibility coefficient, R is the gas constant, and T is the absolute temperature (*13*).

The pressure dependence of the chemical shifts was analyzed according to

$$\delta_i = a_i + b_i p + c_i p^2 \quad (4)$$

where δ_i is the chemical shift for the ith residue, and a_i, b_i, and c_i are independent linear and nonlinear coefficients of the pressure-induced shift, respectively.

Curve fitting was performed using SigmaPlot2001 (SPSS Science, Chicago, IL) on all observed data.

RESULTS

Spectral Densities. First, we measured the reduced spectral density function (*18*), $J(\omega)$, for almost all residues of PrP^C, which would provide insights into the motion of the N−H bond vector at five frequencies 0, 0.32, 0.51, 2.73, and 4.37

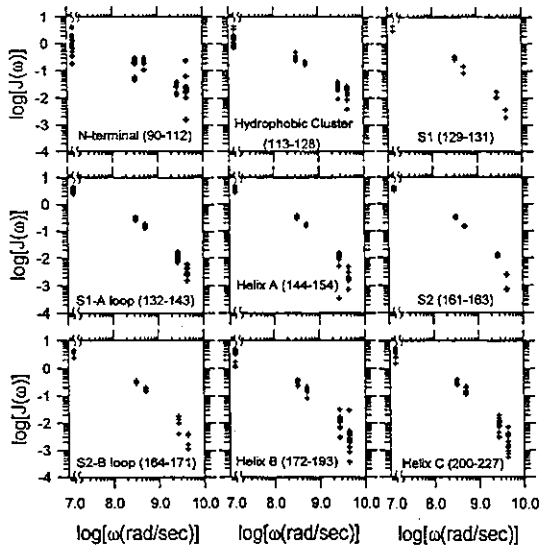

FIGURE 1: The reduced spectral density function, $J(\omega)$, of the N−H bond vector is shown for different regions of PrP^C at five frequencies: 0, ω_{N1} (0.32 grad/s), ω_{N2} (0.51 grad/s), $0.87\omega_{H1}$ (2.73 grad/s), and $0.87\omega_{H2}$ (4.37 grad/s), where subscripts 1 and 2 denote angular velocities at 11.7 and 18.8 T, respectively.

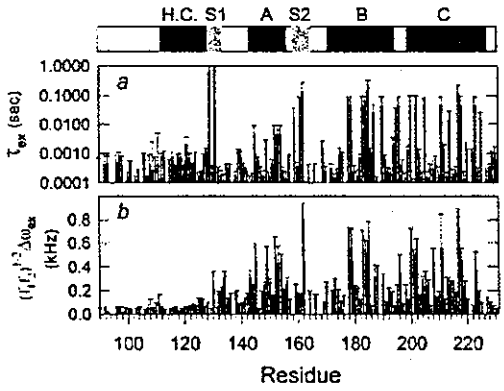

FIGURE 2: (a) Slow exchange lifetimes (τ_{ex}) obtained using the CPMG dispersion method (*14*) plotted as a function of residue number. (b) $\{f_1f_2\}^{1/2}\Delta\omega_{ex}$ plotted as a function of residue number. $\Delta\omega_{ex}$ is the difference in chemical shift of the nucleus in the two conformational states. f_1 and f_2 (= $(1 - f_1)$) are the populations of the two conformational states.

gigaradian (grad)/s using two static magnetic field strengths, 11.7 and 18.8 T. As shown in Figure 1, $J(0)$ values for the N-terminal and hydrophobic cluster are relatively low and rather dispersed, while those for residues in S1 and S2 β-strands and helices B and C are comparatively high. Large $J(0)$ values reflect the global tumbling motion (*12*). We note that J (4.37 grad/s) values are also quite heterogeneous for N-terminal regions and helices B and C, suggesting a large degree of flexibility.

Slow Exchange Dynamics. We obtained evidence of slow conformational exchange from the τ_{cp} dependence of the CPMG dispersion experiments. By assuming two-site exchange, we apply eq 1 (see Materials and Methods) to the CPMG relaxation dispersion data. Figure 2a shows lifetimes corresponding to the slow exchange rates obtained (*14*). Values for the slow exchange time constant, τ_{ex}, and the

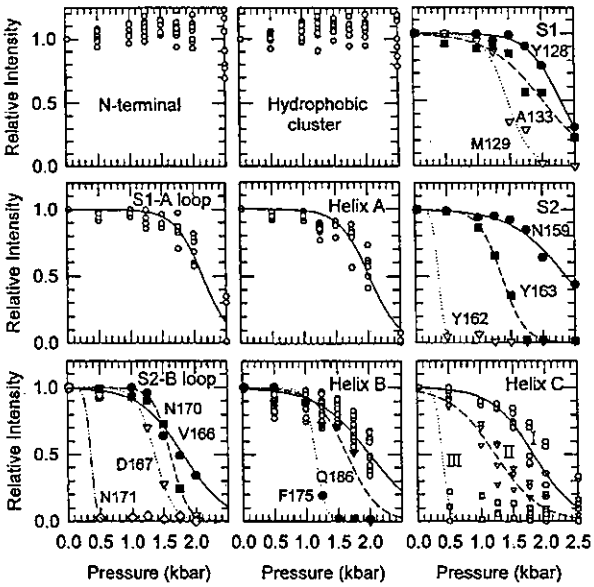

FIGURE 3: Integrated intensities of amide resonances in HSQC spectra as a function of pressure. The transition profiles are divided into nine groups according to secondary structure elements of PrP^C. The multiple values at each pressure correspond to different residues within a structural region. Lines are from curve fitting using eq 2. The transition from the native conformation varies from site to site, showing that the pressure stability of rPrP(90−231) is site-dependent.

difference in chemical shifts ($\Delta\omega$), shown in Figure 2b, were calculated using eq 1. The τ_{ex} values are on the microsecond-to-millisecond time scale, and the relatively large $\Delta\omega$ values are mainly found in the β-strands S1 and S2 and helices B and C. Specifically, residues with τ_{ex} larger than 0.01 s are M129, G131, N159, V161, Y162, D178, C179, T183, I184, L185, H187, T190, G195, E196, E200, D202, I205, E211, C214, Q217, Y218, Q223, and Y225. They are mapped by yellow in Figure 4a.

High-Pressure NMR. Under high pressure, the population of the native state is generally decreased and, if present at all, that of an intermediate state is increased, because the partial molar volume of the native structure is generally larger than that of the intermediate structure, since it is presumably less tightly folded. Pressure-induced conformational transitions are generally less cooperative than those of other perturbations, such as temperature or denaturant concentration, because, in the native conformation, each affected residue is adjacent to a cavity with specific volume. Therefore, pressure-induced disorder of the native conformation often varies from site to site, showing that the thermodynamic stability of rPrP(90−231) is site dependent. We categorized the behaviors of the integrated intensities of amide residues in HSQC spectra as a function of pressure into nine groups according to secondary structure elements of the protein, as shown in Figure 3. Lines are theoretically generated by fitting eq 2, in Materials and Methods, to the experimental data points. Cross-peak intensities from the N-terminus and the hydrophobic cluster were essentially invariant with pressure, while intensities for residues 128−231 dramatically decreased with pressure, almost disappearing by 2500 bar. This indicates that the major conformational changes are occurring. The relative inertness of spectral

features to pressure is a general property of a disordered conformer. There is substantial heterogeneity in pressure stability among the secondary structure elements. The S1-A loop and helix A were most stable with pressure change, and their transitions occurred uniformly over their constituent residues. Pressure-induced transitions of helix B residues also occurred rather uniformly, with the exception of F175 and Q186. The pressure stability is determined mainly by two factors, the stability at 1 bar (ΔG_0) and ΔV, neglecting the $\Delta\beta$ contribution (eq 3). By extrapolating eq 3 to 1 bar and neglecting data for F175 and Q186, we obtain average thermodynamic stabilities ΔG_0 of helix A and helix B at 1 bar to be 5.2 and 3.0 kcal/mol, respectively. The results clearly indicate that helix B has much less stability than helix A. Other secondary structure elements were even less stable against pressure, and their transitions were more heterogeneous. Transitions of residues in β-strands S1 and S2, the S2-B loop and helix C occurred quite heterogeneously at pressures between 500 and 2500 bar. Transitions were most varied for helix C. They are roughly categorized into three groups (see Figure 3); group I (○: composed of most residues), group II (▽; V210, M213, Q217, K220), and group III (□; K204, I205, Q219).

Thermodynamic analysis, extrapolated to 1 bar via eq 2, gave ΔG_0 values of 3.4 kcal/mol for group I and 2.1 kcal/mol for group II. The group II residues are located essentially at the interface with β-strands S1 and S2, suggesting that the apparent low stability arises from increased conformational disorder of these residues relative to strands S1 and S2. K204, I205, Q219 in group III of helix C, Y162 of S2, N171 of the S2-B loop and F175 of helix B were exceptionally unstable and underwent transitions below 1000 bar. Residues M129, Y163, D167, N170, F175, V210, M213, Q217, and K220 exhibited moderate instability and undergo transitions around 1500 bar. They are mapped in magenta and yellow, respectively, on the NMR structure (*11*) in Figure 4b. Although residues with pressure-induced instability are distributed mainly around the interface between S2 and helix C as shown in Figure 4b, those with any significant slow fluctuations with τ_{ex} more than 0.01 s are distributed more widely and cover S1, S2, helices B and C, as shown in Figure 4a.

Correlation between Fluctuation-Induced and Pressure-Induced Chemical Shift Changes. We have compared the fluctuation- and pressure-induced chemical shift changes, since the measurements are not a priori related. Figure 5a is the plot of the chemical shift changes of amide ^{15}N nuclei induced by fluctuation, $\{f_1f_2\}^{1/2}\Delta\omega_{ex}$, with τ_{ex} larger than 1 ms, against the linear components of the pressure dependence of the ^{15}N chemical shifts (*13*). Although the amplitudes of the former are about 10 times larger than the latter, they are reasonably well correlated. On the other hand, there is no evident correlation between the chemical shift changes of amide ^{15}N nuclei induced by slow exchange fluctuations, $\{f_1f_2\}^{1/2}\Delta\omega_{ex}$ with τ_{ex} larger than 1 ms, and any (total or nonlinear) component of the pressure dependence of the ^{15}N chemical shifts (data not shown). Correlations between the chemical shift changes of amide ^{15}N nuclei induced by fluctuation, $\{f_1f_2\}^{1/2}\Delta\omega_{ex}$ with τ_{ex} on the time scale of microsecond and any pressure dependence of the ^{15}N chemical shifts are not evident.

DISCUSSION

Dynamic Features of the Natively Unfolded N-Terminal Region. Since regions in the hydrophobic cluster (113−128) are only transiently folded (*11*), no significant slow dynamics nor any significant conformational transition was observed (Figures 1−3). However, the hydrophobic cluster is apparently necessary for PrP to convert into PrP^{Sc}. For example, transgenic mice with removal of N-terminal residues beyond residue 93 did not support PrP^{Sc} formation. Interestingly, Tg mice expressing PrP(121−231) develop a cerebellar disorder in the neonatal period implying that much, if not all, of the N-terminal moiety of PrP is necessary for normal function (*24*). Deletion of the C-terminal helices also causes a heritable disorder with severe nerve cell loss (*25*). Therefore, we may assume that the hydrophobic cluster functionally lies within the "death domain", which spontaneously forms the killer conformation via intermolecular interactions such as other conformational diseases (*26*), on the condition that this region is accessible to other pertinent molecules.

Hydrogen bonds apparently exist between M129 and Y163 in the small, unstable β-sheet (*11*), so it is not surprising to see in Figure 3 that M129 and Y163 together exhibit a pressure-induced change. The polymorphism of residue 129, being a valine in many humans, results in different disease phenotypes expressed by the D178N mutation shown in Figure 6f, which can be understood in terms of the structure (*11*). Different clinical manifestations and different prion diseases may result from different conformations of PrP^{Sc} being present. The pressure study further indicates that the region of the S1 strand with methionine at residue 129 is inherently unstable. Residue 129 is near D178, with some evidence that the D178 carboxylate is hydrogen bonded to the Y128 ring hydroxyl (*11*), so conformational fluctuations in helix B can propagate into the S1 strand and proximal hydrophobic cluster. Some amides in the ill-formed β-sheet undergo very slow fluctuations (Figures 2 and 6a,b) and are also affected more readily by pressure (Figures 3 and 6c). That is not surprising, as multiple NMR signals were observed for some β-strand residues (*11*). Both observations emphasize that the β-sheet in PrP^{C} is not very stable. Conceivably, the pressure instability of F175 in helix B is also related to comparatively low stability of S2 and S2-B loop.

Slow Dynamics and Stability of the C-Terminal Helical Region. PrP* was first observed as a metastable intermediate during the unfolding process of SHa rPrP(90−231) with guanidinium chloride (*27*). Other observations have supported the existence of intermediate forms of prions (*28, 29*). Recently, we characterized some structural features of PrP* (*13*). A small amount of PrP* coexists with native PrP^{C} under nearly physiological conditions (pH 5.2, 30 °C, 1 bar) with the pressure-dependence studies, suggesting that PrP* has disordered B and C helices, while helix A is largely intact (*13*). From the pressure dependence of the signal intensities of individual residues for PrP^{C}, the stability difference of $\Delta G_0 = 2.1$ kcal/mol was obtained for group II residues. This indicates that as much as 1−3% of PrP exists as PrP* at ambient temperature and pressure. Assuming that the signals observed are all from PrP^{C}, the present relaxation analysis indicates that PrP^{C} undergoes millisecond fluctuations particularly in the vicinity of helices B and C.

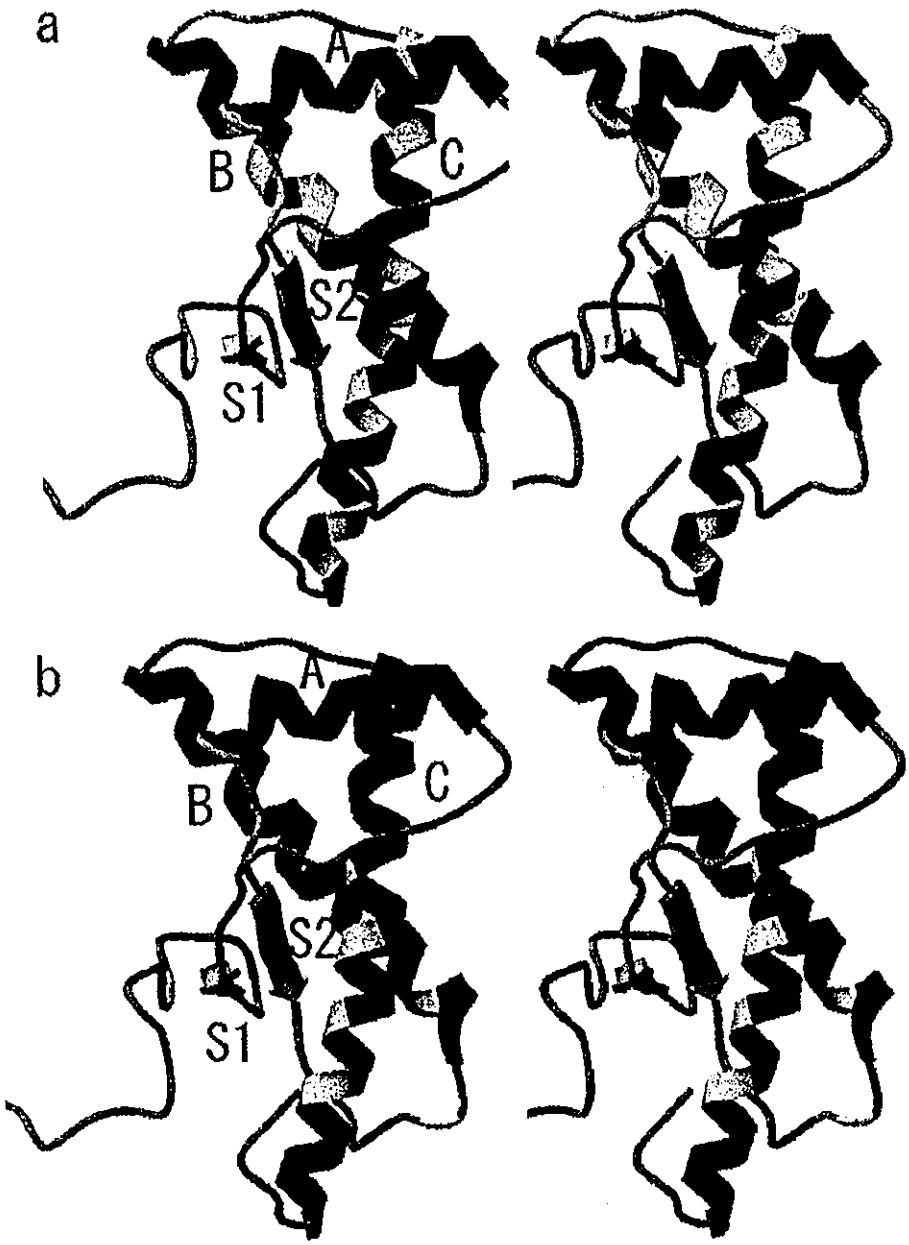

FIGURE 4: In the context of the PrP(90−231) structure, comparison of CPMG T_2 conformational dynamics and high-pressure-induced conformational changes. (a) Residues with τ_{ex} larger than 0.01 s are M129, G131, N159, V161, Y162, D178, C179, T183, I184, L185, H187, T190, G195, E196, E200, D202, I205, E211, C214, Q217, Y218, Q223, Y225, and are mapped in yellow on the NMR structure (*11*). Red represents the helical region, and blue represents other regions. (b) Exceptionally unstable residues that undergo transitions below 1000 bar (K204, I205, Q219 in group III of helix C, Y162 of S2, N171 of the S2-B loop and F175 of helix B), and moderately unstable residues that undergo transitions around 1500 bar (M129, Y163, D167, N170, F175, V210, M213, Q217, and K220) are mapped in magenta and yellow, respectively, on the NMR structure (*11*).

The unstable residues of helices B and C are near a cluster of cavities (*13*), suggesting that the slow dynamics and selective disorder of helices B and C may be related to instability of these cavities. In particular, the HSQC cross-peak intensity reduction observed at relatively low pressures (<500 bar) for group III residue Q219 on helix C is remarkable. As noted previously (*11*), the hamster species, SHa PrP(90−231), and the mouse species, Mo PrP(121−231), differ in that the latter exhibits a break in the helix at Q219. Also, the S2-B loop in SHa PrP (90−231) is well-defined by NMR data but is disordered in Mo PrP (121−231). It should be also noted that Q219 corresponds to the region exhibiting the dominant negative inhibition of prion replication (*26*) (Figure 6d) and also belongs to the protein X binding epitope (*30*) (Figure 6e). Four residues, Q168 in the S2-B loop, Q172 at the beginning of helix B, and T215 and Q219 on helix C, form an epitope that interacts with the putative protein X (*30*), which may well be something other than a protein. Q168, as part of the helical turn, is not in close proximity to the other three residues (Figure 6e).

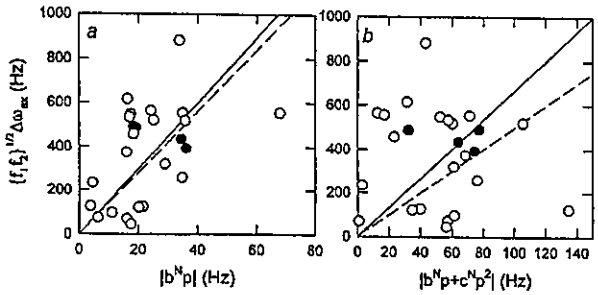

FIGURE 5: Plots of the chemical shift changes of amide ^{15}N nuclei induced by slow fluctuations versus pressure dependencies of the amide ^{15}N chemical shift (*13*). Symbols (○) and (●) indicate residues in helices and in β-sheets, respectively, and lines represent the result of regression analyses. (a) Plot of $\{f_1f_2\}^{1/2}\Delta\omega_{ex}$ for residues with τ_{ex} larger than 1 ms against the linear component of the pressure-dependent chemical shift change of amide ^{15}N resonances. (b) Plot of $\{f_1f_2\}^{1/2}\Delta\omega_{ex}$ for residues with τ_{ex} larger than 1 ms against the total pressure-dependent chemical shift change of amide ^{15}N resonances.

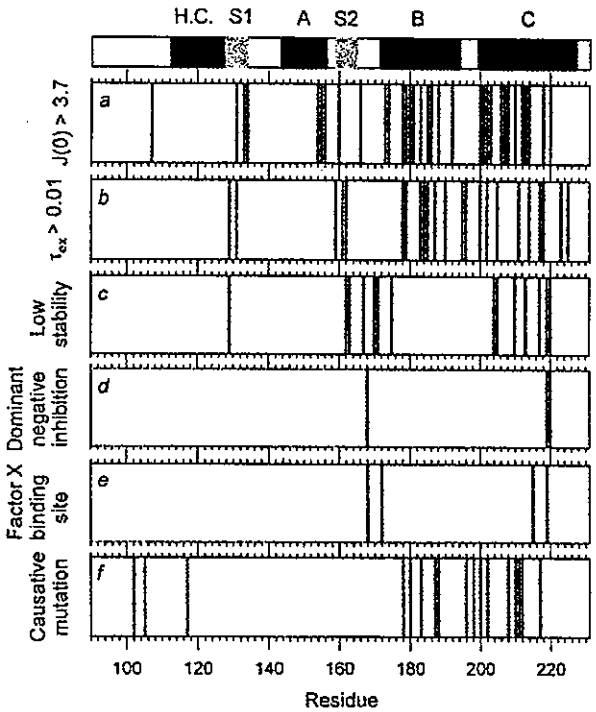

FIGURE 6: Plot of residues whose (a) $J(0)$ values are larger than 3.7 ns, obtained via reduced spectral density mapping, and (b) τ_{ex} values are larger than 0.01 s, obtained using the CPMG method. (c) Residues with low stability detected by high-pressure NMR. (d) Residues with polymorphisms exhibiting dominant negative inhibition of prion replication (*26*). (e) Residues mapped as the protein X binding epitope (*30*). (f) Residues whose mutations cause neurodegenerative diseases in humans.

We can speculate that conformational flexibility in the region facilitates factor X binding.

In PrP^C, slow fluctuations are evidently not connected to observed fast (picosecond-to-nanosecond) fluctuations. Amino acid residues predominantly fluctuating on the millisecond time scale mainly exist in helices B and C, which are also locally disordered in the PrP* intermediate state (*13*). This coincidence suggests that the slow dynamics of the prion protein includes trajectories from the native state to the thermodynamically distinct substate, PrP*. The thermodynamic picture derived from pressure-induced unfolding is not expected from the static NMR structure, nor from the dynamic picture on the picosecond-to-nanosecond time scale, which emphasizes the difference between unstructured N-terminal and structured C-terminal regions (*11*, *12*). Logically, millisecond time scale fluctuations may be qualitatively different from picosecond-to-nanosecond time scale motions (*31*−*33*). The overall coincidence between the stability and the slow dynamics suggests that the slow fluctuations of PrP occur along the reaction surface of the protein folding (*32*). However, the fast motions may just entail low energy fluctuations of the native structure. The curvature of the reaction surface for protein folding may not necessarily correspond to the local energy surface around the native PrP^C structure.

Correlations between Slow Fluctuations under Physiological Conditions and Pressure-Dependent Conformational Changes. The NMR relaxation analysis gives residue-specific amide chemical shift differences between two putative conformers that are considered to be mutually interconverting. These differences should reflect the amplitude of the conformational fluctuation at individual residue sites. On the other hand, from the relation between volume fluctuation and compressibility, pressure-induced chemical shift changes are also correlated with the amplitude of fluctuation at individual residues. As shown in Figure 5a, the chemical shift changes of amide ^{15}N nuclei induced by fluctuation, $\{f_1f_2\}^{1/2}\Delta\omega_{ex}$ with τ_{ex} larger than 1 ms, are correlated with the linear component of the pressure dependency of the ^{15}N chemical shift (*13*). This may suggest that slow fluctuations at ambient pressure are occurring within the basic folded subensemble (*34*). The basic folded subensemble is the "ensemble" of the native conformations with essentially the same compressibility exhibiting the linear pressure-dependent chemical shift changes. When they exhibit any nonlinear behavior, we presume it to be a transition from the basic folded structure to the low-lying excited state (*35*).

The amplitudes of the chemical shift fluctuations are about 10 times larger than those of the pressure-induced chemical shift changes. The average ^{15}N chemical shift difference between 1 and 2.5 kbar is ~0.1 ppm, which corresponds to a ψ angle of ~0.4° (*36*). On the other hand, the fluctuation of the ψ angle obtained by the CPMG relaxation experiment is ~4°, which is basically consistent with the results of many MD simulations (*37*). The Gibbs free energy of a protein is generally defined as a function of pressure (P) and temperature (T). In a thermal denaturation process under constant pressure, the entropic change ($T\Delta S$) is the main driving force, while in pressure denaturation at constant temperature, the volume change ($-P\Delta V$) is the major driving force. However, under approximately physiological conditions, a fluctuation may occur along a direction between them, as shown in Figure 7. The pressure-induced conformational changes emphasize the intermediate conformers with large ΔV, while temperature-induced conformational changes emphasize those with large ΔS. However, if a protein could fluctuate in a P/T plane freely during fluctuations, a small population may have a chance to reach a conformation with higher energy along the trajectories. This dynamic event may occur rarely, either because of the high energetic barrier (fast motion but with low probability) or by following a winding pathway along the rugged surface (slow motion). Either way, populat-